MASS TRANSPORT CONTAMINATION
STUDY

FINAL REPORT

January 1973

LOCKHEED MISSILES & SPACE COMPANY, INC.

HUNTSVILLE RESEARCH & ENGINEERING CENTER

HUNTSVILLE RESEARCH PARK

4800 BRADFORD DRIVE, HUNTSVILLE, ALABAMA
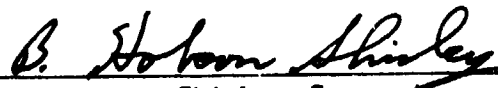
MASS TRANSPORT CONTAMINATION
STUDY

FINAL REPORT

January 1973
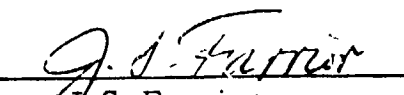
Contract NAS8-26554
Modification 1

by

S. J. Robertson

APPROVED:

B. Hobson Shirley, Supervisor
Aerophysics Section

J. S. Farrior
Resident Director

FOREWORD

This document is the final report for Contract NAS8-26554,
"Mass Transport Contamination Study," Modification 1. The study
was performed by personnel of the Lockheed-Huntsville Research
& Engineering Center for the Space Sciences Laboratory of NASA-
Marshall Space Flight Center. The NASA technical monitor for
the study was Mr. E. E. Klingman, S&E-SSL-PM.

CONTENTS

Section 1
INTRODUCTION AND SUMMARY

This contract was modified on 13 April 1972 to include an extended work statement and period of performance through 13 January 1973. This final report documents results achieved during this extended effort. The additional effort consisted of two tasks, each of which has been separately documented in Lockheed technical reports that are appended to this report. The two tasks are described as: (1) "Backflow of Outgas Contamination onto Orbiting Spacecraft as a Result of Intermolecular Collisions," and (2) "Particle Cloud Buildup Due to Waste Dumping from Orbiting Spacecraft." Both of these tasks deal with aspects of spacecraft contamination in orbit.

Spacecraft contamination is a matter of current and vital interest in the design of thermal control surfaces, solar panels and experiment and instrumentation packages for use aboard earth-orbiting vehicles. Contamination sources include liquid waste dumps, reaction motor firings and material outgassing. The two tasks performed under this contract modification provide analytical techniques with which quantitative estimates can be made of certain specific contamination threats.

Some of the outgas products flowing away from a spacecraft will be deflected back onto the spacecraft as a result of intermolecular collisions. This is particularly true with respect to collisions with ambient atmospheric molecules. Under Task 1, analytical techniques were developed to predict the amount of mass that will return. For the Skylab spacecraft, it was estimated that on the order of 1 or 2% of the outgas products will return to the spacecraft as a result of intermolecular collisions.

Mass dumped overboard from liquid waste dumps will leave the spacecraft and go into orbit about the central body (Earth, Moon, etc.) in much the

same fashion as the spacecraft. The effect of continuing waste dumps is to create a particle cloud in orbit that continuously expands along the spacecraft orbit. Some of this mass will return to the spacecraft at points where the particle orbits intersect the spacecraft orbit. It was estimated for the Skylab spacecraft, neglecting aerodynamic drag, that a particle cloud will extend, on both sides of the spacecraft, about 36 km in the radial direction, 9 km in the out-of-plane direction and will expand along the spacecraft orbit at the rate of 168 km for each spacecraft orbit. Aerodynamic drag will cause the particle cloud to spiral inward toward the central body. Again neglecting aerodynamic drag, the estimated amount of return mass flow was found to be about of the same order as a typical spacecraft material outgas rate. When aerodynamic drag was considered, it was found that particle collisions with the spacecraft were impossible, and the return mass flow rate was, therefore, zero. The predicted light scattering properties of the optical cloud were found to be nearly identical with those predicted for an isotropic source, with some intensification in directions along the spacecraft orbit.

2

Section 2
DISCUSSION AND CONCLUDING REMARKS

The results of the Task 1 effort, "Backflow of Outgas Contamination onto Orbiting Spacecraft as a Result of Intermolecular Collisions," is documented in Ref. 1 and is included in this final report as Appendix A. As pointed out in Appendix A, the treatment of backscattering due to collisions between outflow molecules and atmospheric molecules is considered to be fairly rigorous. The treatment involving collisions between individual outgas molecules, however, is based on somewhat extreme simplifications. Although the backflow due to self-scattering was found to be small for the Skylab spacecraft, future applications might make worthwhile an effort to develop a more rigorous treatment.

The second task, "Particle Cloud Buildup Due to Waste Dumping from Orbiting Spacecraft," is documented in Ref. 2 and is included in this final report as Appendix B. There are a number of areas where this study might be expanded. In the calculations of the particle cloud buildup, it was assumed that the expulsion rate was continuous and uniformly distributed in all directions. It was further assumed that the particle size and velocity distributions were uniform and constant with respect to time. A worthwhile future effort would be to remove some of these restrictions and also to consider the long-term interaction and thermal equilibrium of these particles with the ambient atmosphere.

3

REFERENCES

1. Robertson, S. J., "Backflow of Outgas Contamination onto Orbiting Space-craft as a Result of Intermolecular Collisions," LMSC-HREC D306000, Lockheed Missiles & Space Company, Huntsville, Ala., June 1972.

2. Robertson, S. J., "Particle Cloud Buildup Due to Waste Dumping from Orbiting Spacecraft," LMSC-HREC D306222, Lockheed Missiles & Space Company, Inc., Huntsville, Ala., December 1972.

APPENDIX A

to LMSC-HREC TR D306352

LOCKHEED MISSILES & SPACE COMPANY INC.

HUNTSVILLE RESEARCH & ENGINEERING CENTER

HUNTSVILLE RESEARCH PARK

4800 BRADFORD DRIVE, HUNTSVILLE, ALABAMA

BACKFLOW OF OUTGAS
CONTAMINATION ONTO ORBITING
SPACECRAFT AS A RESULT
OF INTERMOLECULAR COLLISIONS

June 1972
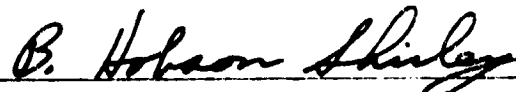
Contract NAS8-26554

by

S.J. Robertson
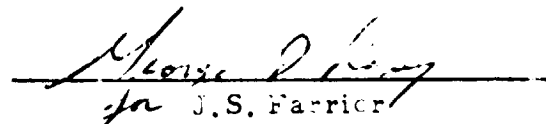
APPROVED:

B. Hobson Shirley, Supervisor
Aerophysics Section

George D. Reny, Manager
Aeromechanics Dept.

for J.S. Farrier
Resident Director

FOREWORD

This interim report documents the results accomplished during performance of Task A of Contract NAS8-26554, "Mass Transport Contamination Study," Modification 1. The work was performed by personnel in the Aeromechanics Department of the Lockheed-Huntsville Research & Engineering Center under Contract to NASA-Marshall Space Flight Center. The MSFC technical monitor for the contract is E.E. Klingman, S&E-SSL-PM.

CONTENTS

Section 1
INTRODUCTION AND SUMMARY

Orbiting space vehicles lose mass to the ambient environment as a re-
sult of outgassing of spacecraft materials, dumping of waste products and
firing of attitude control reaction motors. Some of the lost mass will return
to the vehicle, where even very small amounts may significantly cloud space-
craft windows, contaminate experiment packages or otherwise interfere with
spacecraft operations.

In the highly rarefied environment at orbital altitudes, backscattering
due to intermolecular collisions will be a primary mode by which outgas
products will be deflected back onto the vehicle. The intermolecular collisions
will be of two distinct types. First, they will occur between the outflowing
molecules and the ambient atmospheric molecules. The stream of ambient
atmospheric molecules will be highly energetic, corresponding to the orbital
velocity of the spacecraft. Intermolecular collisions of this type will conse-
quently tend to strongly deflect the outflowing molecules in the direction of the
ambient freestream. Second, intermolecular collisions will occur between
individual outflowing molecules because of differences in velocity (including
direction) of the individual molecules.

To provide an indication of the amount of backflow to be expected, a
theoretical analysis was performed based on the following simplifying assump-
tions. The spacecraft was assumed to be spherical in shape with the mass
flow emitting uniformly over the spherical surface at a constant rate and in a
D'Lambertian spatial distribution. The outflow gases were assumed to be
neutrally charged and of a single species with a molecular weight character-
istic of a composite of the actual species involved in the mass flow.

The theoretical analysis showed that, for outgassing only, less than 1.5% of the outgas products will return to the Skylab spacecraft as a result of inter-molecular collisions. When the total mass flow from the spacecraft, including waste dumps, reaction control motor firings, etc., was considered, it was estimated that about 30% will return to the spacecraft. The latter result is based on certain rather extreme simplifying assumptions.

Section 2

METHOD OF APPROACH AND DERIVATION OF EQUATIONS

2.1   METHOD OF APPROACH

The highly rarefied environment under consideration is such that the
flow may be considered to be "nearly free molecular." In this flow regime,
the mean free-path between intermolecular collisions is large compared to
typical spacecraft dimensions, yet small enough to cause significant departure
from free molecular flow. The fact that the flow regime is indeed nearly free
molecular will be shown later for the Skylab spacecraft.

In this flow regime, the "first-collision" model approach of Baker and
Charwat (Ref. 1) is appropriate. Each molecule is considered to undergo a
maximum of one intermolecular collision prior to colliding with a surface, or
between two successive collisions with a surface. In the present applications,
this allows two classes of collisions to be considered: (1) between an outflowing
molecule and an ambient atmospheric molecule, neither of which has undergone
previous collisions; and (2) between two outflowing molecules which have not
experienced prior collisions. Collisions between ambient atmospheric mole-
cules are neglected altogether since the frequency of such collisions is ex-
tremely small compared to that of the other two classes of collisions. Actually,
Baker and Charwat considered only class (1) collisions. Since it is difficult to
show that class (2) collisions are in fact negligible (Ref. 2), they will be con-
sidered in this analysis by using certain simplifying assumptions.

The first-collision approach considers the molecules to be smooth, hard
elastic spheres of some finite diameter. In the present analysis, the diameter
is made flexible depending on the relative velocity between collisions to account
for realistic temperature variations in viscosity.

2-1

2.2 DERIVATION OF EQUATIONS

It is necessary first to determine the collision rate per unit volume that occurs in the region surrounding the sphere. Next, a determination is made of the number of colliding outflow molecules in an element of volume which are deflected back in the direction of a given point on the surface. The total back-flow flux at the given point is then determined by integrating over the half space outward from the point on the surface. This is described separately for the two classes of collisions in the following paragraphs.

2.2.1 Scattering by Ambient Atmospheric Molecules

Consider the geometrical representation shown in Fig. 1. The point on the sphere surface at which the backflow flux is to be calculated is designated Q, while a point in the field surrounding the sphere which is a source of back-scattered molecules is designated P. For convenience Q is considered to be in the $\vec{i}, \vec{j}$ plane, where $\vec{i}, \vec{j}$ and $\vec{k}$ are unit vectors in the direction of corresponding rectangular coordinates with $\vec{i}$ pointing in the negative direction of the ambient flow. The angle ϕ is the latitudinal displacement from the $\vec{i}$ axis. In the primed coordinate system, $\vec{i}'$ is in the direction of the radius passing through Q, $\vec{j}'$ is in the $\vec{i}, \vec{j}$ plane and $\vec{k}'$ is in the $\vec{k}$ direction. ϕ' and θ' are polar coordinates about the $\vec{i}'$ axis. Finally, r is the distance from the sphere center out to P, while r' is the distance from Q to P.

The collision rate per unit volume, $\dot{n}$, in the field surrounding the sphere is given by:

$$\dot{n} = n_e n_\infty |\vec{V}_\infty - \vec{v}_e| \sigma_{e-\infty} \tag{1}$$

where n_e is the density field of outflow molecules, n_∞ is the density of the ambient atmosphere, $\vec{V}_\infty$ is the ambient flow velocity, $\vec{v}_e$ is the velocity of the outflow molecules and $\sigma_{e-\infty}$ is the cross section for collisions between the outflow molecules and the ambient atmospheric molecules.
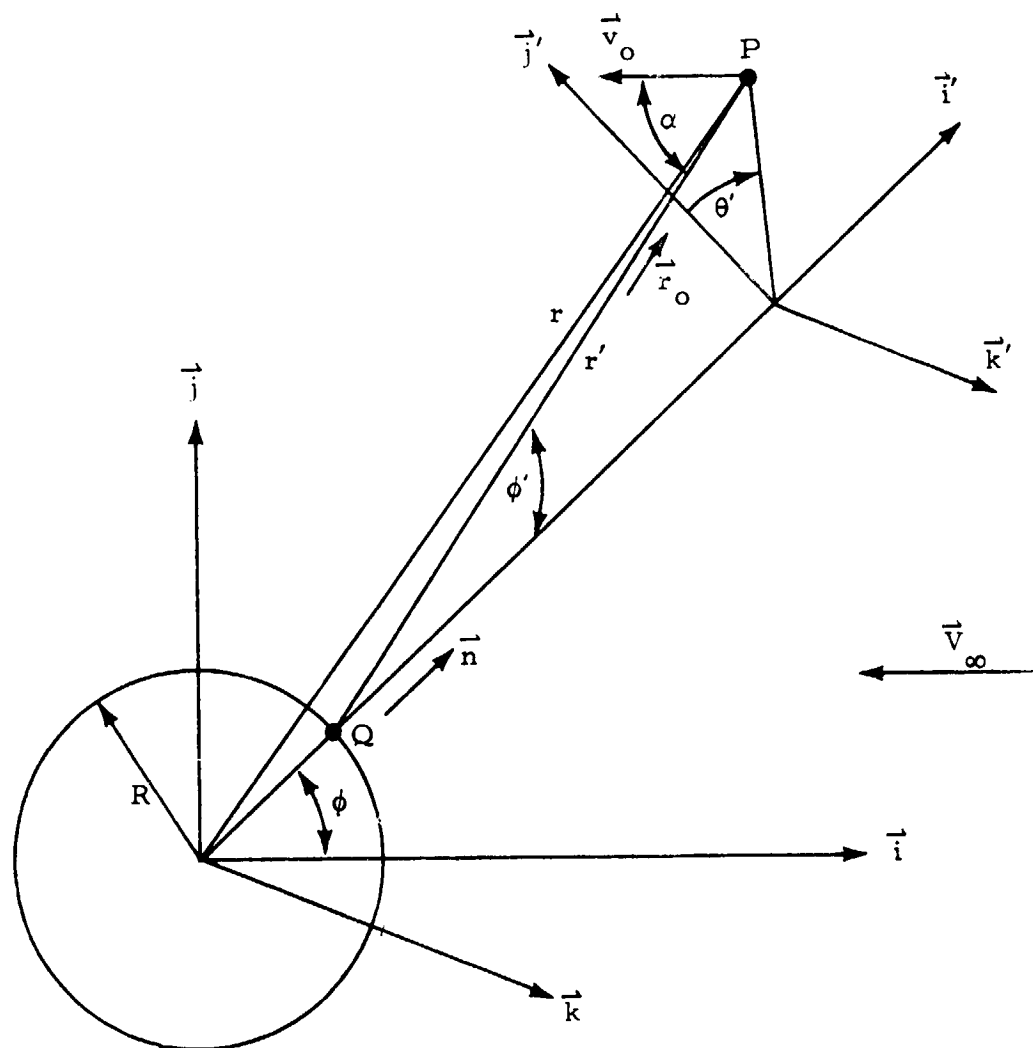
2-2

Fig. 1 - Geometrical Representation of Scattering by Ambient
Atmospheric Molecules

The density field n_e of outflowing molecules at P is determined by

$$n_e = \int_\Omega \frac{q_w}{\overline{v}_w} \frac{d\omega}{\pi} \tag{2}$$

where q_w is the outflow flux at the sphere surface, $\overline{v}_w$ is the mean velocity of the outflow molecules and the integration is over the solid angle ω subtended by the sphere at P. We assume here that the variation in the density field is due entirely to the diverging flow away from the sphere, and that attenuation due to collisions may be neglected. This assumption is justified by the mean free-path being much larger than the sphere radius, as is shown later for the Skylab spacecraft.

Carrying out the integration in Eq. (2) yields

$$n_e = \frac{2\, q_w}{\overline{v}_w} \frac{r - \sqrt{r^2 - R^2}}{r} \tag{3}$$

Referring again to Eq. (1), $\dot{n}$ is seen to be given by

$$\dot{n} = \frac{2\, q_w\, n_\infty\, \left|\overline{V}_\infty - \overline{v}_e\right|\, \sigma_{e-\infty}}{\overline{v}_w} \frac{r - \sqrt{r^2 - R^2}}{r} \tag{4}$$

Next, the directional distribution must be determined of scattering of those outflow molecules undergoing collisions in an element of volume at P. To do this, the velocity of the outflow molecules is assumed to be negligible compared to the velocity of the ambient atmospheric molecules. The outflow molecules may then be considered stationary with respect to the sphere. Consider the hard sphere collision shown schematically in Fig. 2. For all collisions in which the line of centers is in the solid angle element $d\omega$, the stationary molecule will be deflected into $d\omega$ on the opposite side of the stationary molecule. The probability dP_ω of the line of centers lying in $d\omega$ is given by the amount of sphere surface contained in $d\omega$ projected in the direction of flow ratioed to
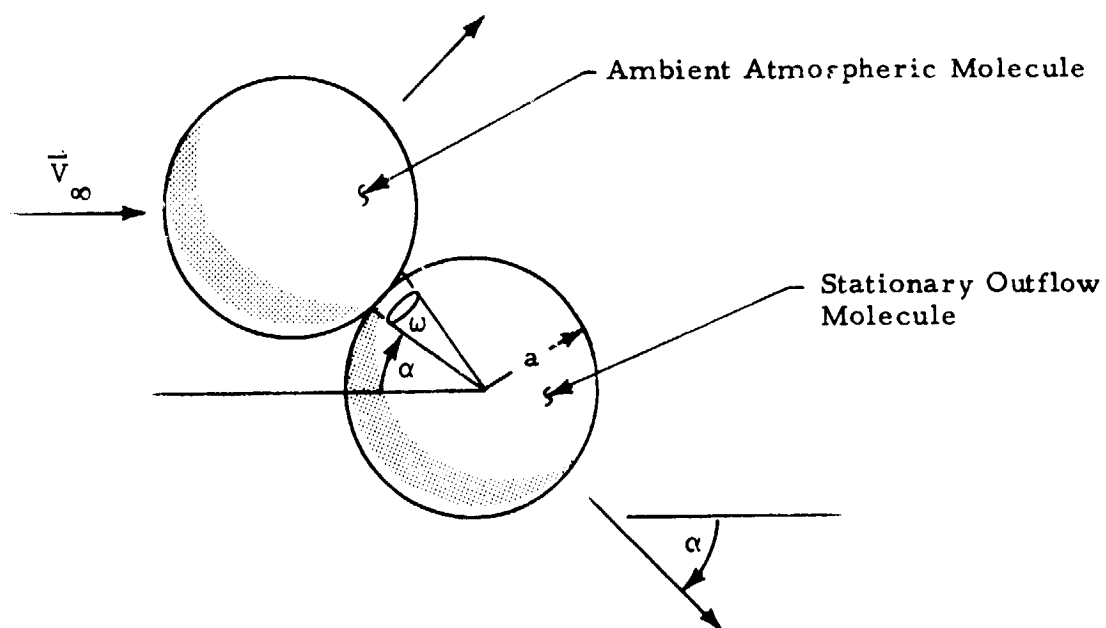
2-4

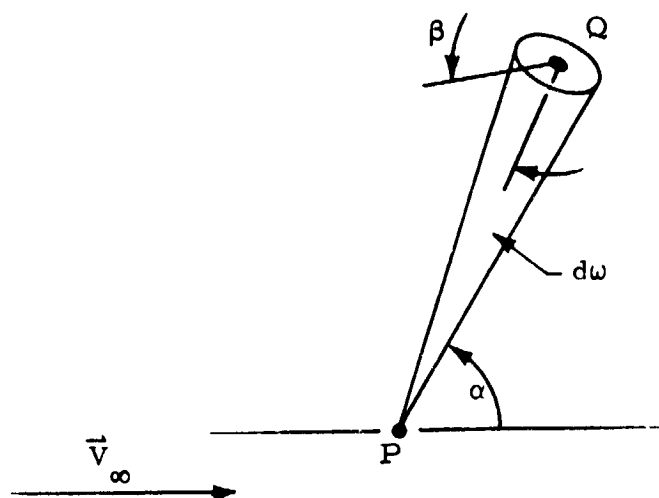Fig. 2 - Schematic of Hard Sphere Collision

Fig. 3 - Diagram for Scattered Flux Due to Collisions

2-5

the sphere cross section:

$$dP_\omega = \frac{a^2\,d\omega}{\pi\,a^2}\cos\alpha = \frac{\cos\alpha}{\pi}\,d\omega \tag{5}$$

Now, referring to Fig. 3, the flux dq_b is found of scattered outflow molecules from collisions in volume element dV at P and crossing surface element dA at Q. Surface element dA is oriented at angle β to the line joining P and Q, and Q is at a distance r' from P.

$$dq_b = \frac{\dot{n}\,dV\,\frac{\cos\alpha}{\pi}\,d\omega}{r'^2\,d\omega}\cos\beta = \frac{\dot{n}\,\cos\alpha\,\cos\beta}{\pi\,r'^2}\,dV \tag{6}$$

Referring again to Fig. 1, the flux dq_b of backscattered outflow molecules at Q is

$$q_b = \frac{2\,q_w\,n_\infty\,V_\infty\,\sigma_{e-\infty}}{\pi\,\bar{v}_w}\int \frac{\cos\alpha\,\cos\phi'}{r'^2}\left(\frac{r - \sqrt{r^2 - R^2}}{r}\right)dV \tag{7}$$

where the volumetric integral is carried out over the portion of the half space outward from dA at Q which is also forward of Q in the negative direction of the external flow (recall from Fig. 2 that molecules are scattered only in the forward direction).

Before Eq. (7) is evaluated for arbitrary ϕ, the integration is performed at $\phi = 0$ and at $\phi = \pi/2$.

$$\frac{q_{b,o}}{q_w} = \frac{4\,n_\infty\,V_\infty\,\sigma_{e-\infty}}{\bar{v}_w}\int_o^{\pi/2}\cos^2\phi'\,\sin\phi'\int_o^\infty\left(\frac{r - \sqrt{r^2 - R^2}}{r}\right)dr'\,d\phi' \tag{8}$$

The radial distance r under the r' integral sign is a function of r' and ϕ' as follows

$$r = (R^2 + 2\cos\phi'\,r'\,R + r'^2)^{1/2} \tag{9}$$

2-6

The difficulty of performing the integration is lessened greatly by approximating the expression under the r' integral sign by the following simpler expression:

$$\frac{r - \sqrt{r^2 - R^2}}{r} \cong \frac{1}{2}\left(\frac{R^2}{r^2} + \frac{R^6}{r^6}\right) \tag{10}$$

The close agreement between the two expressions is shown in Fig. 4.

Equation (8) now becomes

$$\frac{q_{b,o}}{q_w} = \frac{2\,n_\infty\,V_\infty\,\sigma_{e-\infty}\,R}{\overline{v}_w}\int_0^{\pi/2}\cos^2\phi'\,\sin\phi'$$

$$\times\left(\int_0^\infty\frac{d\tilde{r}'}{1 + 2\cos\phi'\,\tilde{r}' + \tilde{r}'^2} + \int_0^\infty\frac{d\tilde{r}'}{\left(1 + 2\cos\phi'\,\tilde{r}' + \tilde{r}'^2\right)^3}\right)d\phi' \tag{11}$$

where $\tilde{r}' = r'/R$. The group of constant factors preceding the integral signs may be rearranged and expressed in terms of certain dimensionless parameters widely used in rarefied gas dynamics:

$$\frac{2\,n_\infty\,V_\infty\,\sigma_{e-\infty}\,R}{\overline{v}_w} = \sqrt{\frac{\pi}{2}}\,\frac{S_b}{Kn}\,\frac{\sigma_{e-\infty}}{\sigma_\infty} \tag{12}$$

where S_b is the ambient velocity ratioed to the most probable thermal velocity of the outflow molecules at the surface temperature, Kn is the ambient mean free-path ratioed to the sphere radius, and $\sigma_{e-\infty}/\sigma_\infty$ is the cross section for collisions between outflow molecules and ambient atmospheric molecules ratioed to the cross section for collisions between individual ambient atmospheric molecules.
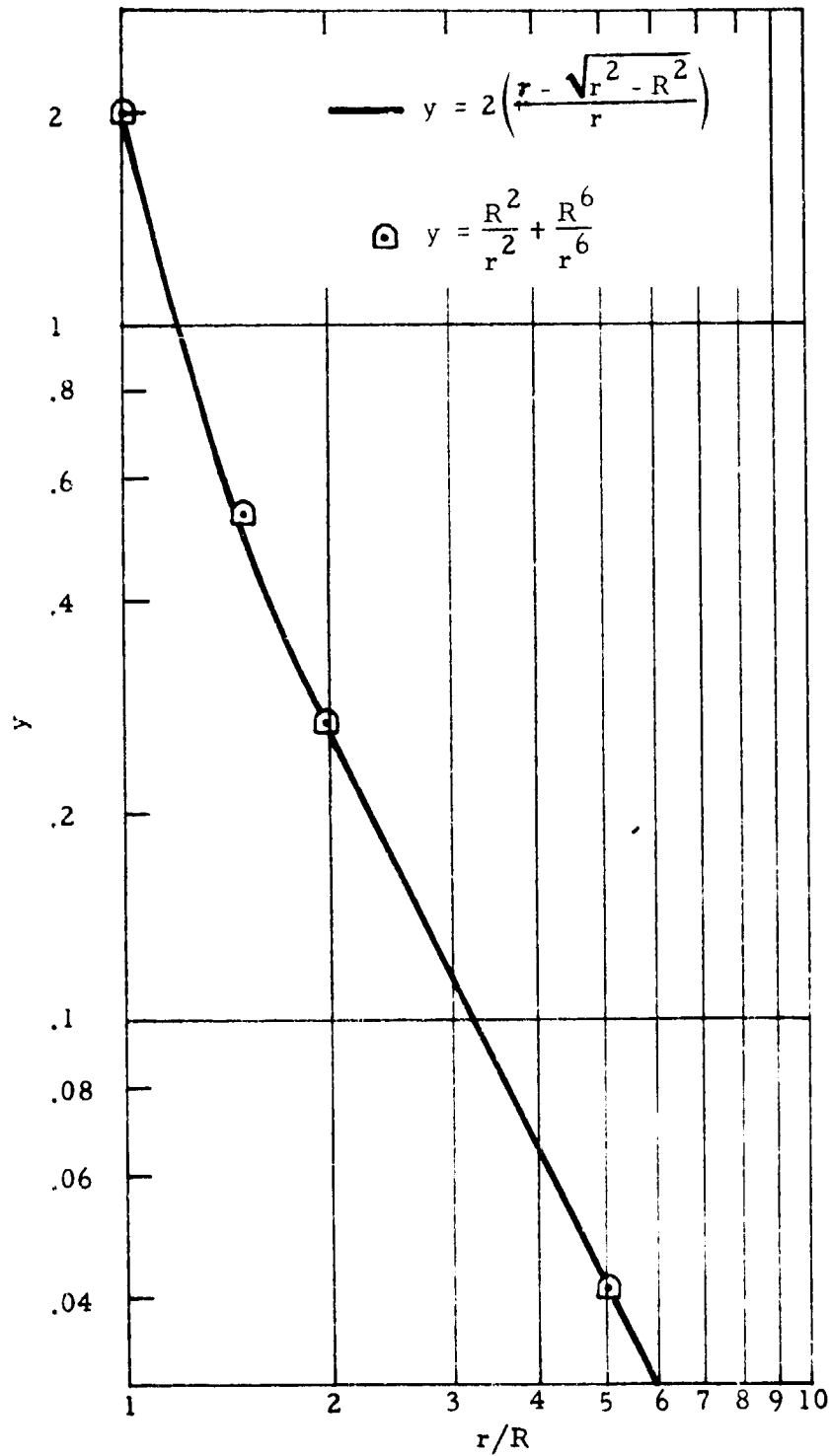
2-7

Fig. 4 - Approximate Expression $R^2/r^2 + R^6/r^6$ Compared to Exact Expression $2(r - \sqrt{r^2 - R^2})/r$

2-8

The integrals over $\widetilde{r}'$ in Eq. (11) are given as follows:

$$\int_0^\infty \frac{d\widetilde{r}'}{1 + 2\cos\phi\,\widetilde{r}' + \widetilde{r}'^2} = \frac{\phi'}{\sin\phi'} \tag{13}$$

$$\int_0^\infty \frac{d\widetilde{r}'}{\left(1 + 2\cos\phi\,\widetilde{r}' + \widetilde{r}'^2\right)^3} = \frac{3\phi'}{8\sin^5\phi'} - \frac{\cos\phi'}{4\sin^2\phi'} - \frac{3\cos\phi'}{8\sin^4\phi'} \tag{14}$$

Equation (11) now becomes:

$$\frac{q_{b,0}}{q_w} = \sqrt{\frac{\pi}{2}} \frac{S_b}{Kn} \frac{\sigma_{e-\infty}}{\sigma_\infty} \left\{ \int_0^{\pi/2} \phi'\cos^2\phi'\,d\phi' + \frac{3}{8}\int_0^{\pi/2} \frac{\phi'\cos^2\phi'}{\sin^4\phi'}\,d\phi' \right.$$

$$\left. - \frac{1}{4}\int_0^{\pi/2} \frac{\cos^3\phi'}{\sin\phi'}\,d\phi' - \frac{3}{8}\int_0^{\pi/2} \frac{\cos^3\phi'}{\sin^3\phi'}\,d\phi' \right\}$$

$$= \frac{3\pi^2 - 8}{48} \sqrt{\frac{\pi}{2}} \frac{S_b}{Kn} \frac{\sigma_{e-\infty}}{\sigma_\infty} \tag{15}$$

For $\phi = \pi/2$, making use of the results of Eqs. (10) and (12) through (14), Eq. (7) becomes:

$$\frac{q_{b,\pi/2}}{q_w} = \frac{1}{\sqrt{2\pi}} \frac{S_b}{Kn} \frac{\sigma_{e-\infty}}{\sigma_\infty} \int_0^{\pi/2} \cos\theta\,d\theta \int_0^{\pi/2} \sin\phi'\cos\phi'$$

$$\times \left\{ \phi' + \frac{3}{8}\frac{\phi'}{\sin^4\phi'} - \frac{1}{4}\frac{\cos\phi'}{\sin\phi'} - \frac{3}{8}\frac{\cos\phi'}{\sin^3\phi'} \right\} d\phi' = \frac{5}{32}\sqrt{\frac{\pi}{2}} \frac{S_b}{Kn} \frac{\sigma_{e-\infty}}{\sigma_\infty} \tag{16}$$

or

$$\frac{q_{b,\pi/2}}{q_{b,0}} = \frac{15}{2(3\pi^2 - 8)} = 0.3471 \tag{17}$$

2-9

For general ϕ, the integration of Eq. (7) becomes much more tedius. The angle α is expressed in terms of ϕ, ϕ' and θ' as follows:

$$\alpha = \cos^{-1}(\cos\phi\cos\phi' - \sin\phi\sin\phi'\cos\theta') \tag{18}$$

Recall that the volumetric integral in Eq. (7) is carried out over the portion of the half space forward of Q in the negative direction of the external flow. This is equivalent to requiring that $0 \le \alpha \le \pi/2$. For $0 \le \phi \le \pi/2$, Eq. (7) becomes:

$$
\frac{q_b}{q_w} = \frac{1}{\sqrt{2\pi}}\frac{S_b}{Kn}\frac{\sigma_{e-\infty}}{\sigma_\infty}\left\{\int_0^{\frac{\pi}{2}-\phi}\int_0^\pi (\cos\phi\cos\phi' - \sin\phi\sin\phi'\cos\theta')\cos\phi'\right.
$$

$$
\times \left(\phi' + \frac{3}{8}\frac{\phi'}{\sin^4\phi'} - \frac{1}{4}\frac{\cos\phi'}{\sin\phi'} - \frac{3}{8}\frac{\cos\phi'}{\sin^3\phi'}\right)d\theta'\,d\phi'
$$

$$
+ \int_{\frac{\pi}{2}-\phi}^{\pi/2}\int_{\cos^{-1}\frac{1}{\tan\phi\tan\phi'}}^\pi (\cos\phi\cos\phi' - \sin\phi\sin\phi'\cos\theta')\cos\phi'
$$

$$
\left.\times \left(\phi' + \frac{3}{8}\frac{\phi'}{\sin^4\phi'} - \frac{1}{4}\frac{\cos\phi'}{\sin\phi'} - \frac{3}{8}\frac{\cos\phi'}{\sin^3\phi'}\right)d\theta'\,d\phi'\right\} \tag{19}
$$

Performing the integrations over θ' reduces Eq. (19) to:

$$
\frac{q_b}{q_w} = \frac{1}{\sqrt{2\pi}}\frac{S_b}{Kn}\frac{\sigma_{e-\infty}}{\sigma_\infty}
$$

$$
\times \left\{\pi\cos\phi\int_0^{\pi/2}\cos^2\phi'\left(\phi' + \frac{3}{8}\frac{\phi'}{\sin^4\phi'} - \frac{1}{4}\frac{\cos\phi'}{\sin\phi'} - \frac{3}{8}\frac{\cos\phi'}{\sin^3\phi'}\right)d\phi'\right.
$$

$$
- \cos\phi\int_{\frac{\pi}{2}-\phi}^{\pi/2}\cos^{-1}\frac{1}{\tan\phi\tan\phi'}\cos^2\phi'\left(\phi' + \frac{3}{8}\frac{\phi'}{\sin^4\phi'} - \frac{1}{4}\frac{\cos\phi'}{\sin\phi'} - \frac{\cos\phi'}{\sin^3\phi'}\right)d\phi
$$

$$+ \cos\phi \int_{\frac{\pi}{2}-\phi}^{\pi/2} \sqrt{\tan^2\phi \, \tan^2\phi' - 1} \, \cos^2\phi' \left(\phi' + \frac{3}{8}\frac{\phi'}{\sin^4\phi'} - \frac{1}{4}\frac{\cos\phi'}{\sin\phi'} - \frac{3}{8}\frac{\cos\phi'}{\sin^3\phi'}\right) d\phi' \Bigg\} \quad (20)$$

The first integral in Eq. (20) is identical to the integral in Eq. (15):

$$\int_{o}^{\pi/2} \cos^2\phi' \left(\phi' + \frac{3}{8}\frac{\phi'}{\sin^4\phi'} - \frac{1}{4}\frac{\cos\phi'}{\sin\phi'} - \frac{3}{8}\frac{\cos\phi'}{\sin^3\phi'}\right) d\phi' = \frac{3\pi^2 - 8}{48} \quad (21)$$

After some algebraic manipulation is performed, and expressing in terms of the flux at $\phi = 0$, Eq. (20) then becomes:

$$\frac{q_b}{q_{b,o}} = \Bigg\{ \cos\phi + \frac{48}{\pi(3\pi^2 - 8)} \sin\phi \int_{\frac{\pi}{2}-\phi}^{\pi/2} \left[\sqrt{1 - \frac{\tan^2(\frac{\pi}{2}-\phi')}{\tan^2\phi}} - \frac{\tan(\frac{\pi}{2}-\phi')}{\tan\phi} \cos^{-1}\frac{\tan(\frac{\pi}{2}-\phi')}{\tan\phi} \right]$$

$$\times \sin\phi' \cos\phi' \left(\phi' + \frac{3}{8}\frac{\phi'}{\sin^4\phi'} - \frac{1}{4}\frac{\cos\phi'}{\sin\phi'} - \frac{3}{8}\frac{\cos\phi'}{\sin^3\phi'}\right) d\phi' \Bigg\} \quad (22)$$

To allow integration in closed form, the first factor under the integral sign is approximated as follows:

$$\sqrt{1 - \frac{\tan^2(\frac{\pi}{2}-\phi')}{\tan^2\phi}} - \frac{\tan(\frac{\pi}{2}-\phi')}{\tan\phi} \cos^{-1}\frac{\tan(\frac{\pi}{2}-\phi')}{\tan\phi}$$

$$\cong 1 - \frac{\pi}{2}\frac{\tan(\frac{\pi}{2}-\phi')}{\tan\phi} + (\frac{\pi}{2} - 1)\frac{\tan^2(\frac{\pi}{2}-\phi')}{\tan^2\phi} \quad (23)$$

The approximation was obtained by fitting the quadratic equation to match end points at $x = \tan(\frac{\pi}{2}-\phi')/\tan\phi' = 0$ and 1 and the first derivative at $x = 0$.

Very close agreement between the exact and approximate expressions is shown in the comparison in Fig. 5.

Equation (22) may now be expressed as follows:

$$\frac{q_b}{q_{b,o}} = \left\{ \cos\phi + \frac{48}{\pi(3\pi^2 - 8)} \left[\sin\phi \int_{\frac{\pi}{2}-\phi}^{\pi/2} \sin\phi' \cos\phi' \right. \right.$$

$$\times \left(\phi' + \frac{3}{8} \frac{\phi'}{\sin^4\phi'} - \frac{1}{4} \frac{\cos\phi'}{\sin\phi'} - \frac{3}{8} \frac{\cos\phi'}{\sin^3\phi'} \right) d\phi'$$

$$- \frac{\pi}{2} \cos\phi \int_{\frac{\pi}{2}-\phi}^{\pi/2} \cos^2\phi' \left(\phi' + \frac{3}{8} \frac{\phi'}{\sin^4\phi'} - \frac{1}{4} \frac{\cos\phi'}{\sin\phi'} - \frac{3}{8} \frac{\cos\phi'}{\sin^3\phi'} \right) d\phi'$$

$$\left. \left. + (\frac{\pi}{2} - 1) \frac{\cos^2\phi}{\sin\phi} \int_{\frac{\pi}{2}-\phi}^{\pi/2} \frac{\cos^3\phi'}{\sin\phi'} \left(\phi' + \frac{3}{8} \frac{\phi'}{\sin^4\phi'} - \frac{1}{4} \frac{\cos\phi'}{\sin\phi'} - \frac{3}{8} \frac{\cos\phi'}{\sin^3\phi'} \right) d\phi' \right] \right\} \quad (24)$$

The first integral is seen to be identical to the integral in Eq. (16) for $\phi = \pi/2$, while the other two integrals drop out due to the $\cos\phi$ factors. Also, all three integrals drop out at $\phi = 0$ due to the identity of the limits of integrations, leaving the first term equal to unity. At $\phi = 0$ and $\pi/2$, therefore, Eq. (24) reduces to the previous results for those particular points.

Carrying out the integrations in Eq. (24) yields:

$$\frac{q_b}{q_{b,o}} = \left\langle \cos\phi + \frac{48}{\pi(3\pi^2 - 8)} \left| \frac{\sin\phi}{2} \left[(\frac{\pi}{2} - \phi) \sin^2\phi + \phi \right. \right. \right.$$

$$\left. - \frac{1}{8} \sin2\phi + \frac{3}{8} (\frac{\pi}{2} \tan^2\phi - \frac{\phi}{\cos^2\phi} - \tan\phi) \right]$$

2-12

$$y = \sqrt{1 - x^2} - x \cos^{-1} x$$

$$\bigcirc \quad y = 1 - \pi/2\, x + \left(\frac{\pi}{2} - 1\right) x^2$$
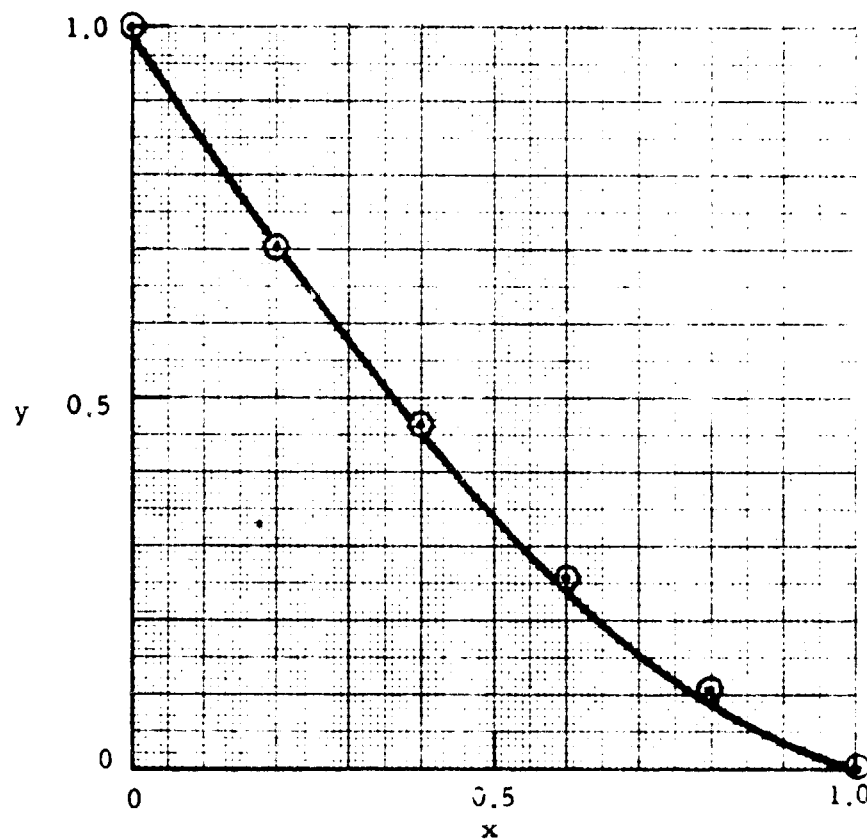

Fig. 5 - Approximate Expression $1 - \frac{\pi}{2} x + \left(\frac{\pi}{2} - 1\right) x^2$ Compared to Exact Expression $\sqrt{1 - x^2} - x \cos^{-1} x$

2-13

$$-\frac{\pi}{8}\cos\phi\left[\pi\phi - (\frac{\pi}{2}-\phi)\sin 2\phi - \phi^2 - \frac{1}{2}\sin^2\phi + \frac{1}{2}\tan^2\phi\left((\frac{\pi}{2}-\phi)\tan\phi - 1\right)\right]$$

$$+ (\frac{\pi}{2}-1)\frac{\cos^2\phi}{\sin\phi}\left[\frac{1}{32}\left(3(\frac{\pi}{2}-\phi)\tan^4\phi - 3\tan^3\phi + \tan\phi\right.\right.$$

$$\left.\left.+ 2\sin 2\phi - 5\phi\right) - (\frac{\pi}{2}-\phi)\ln\cos\phi - \frac{1}{2}(\frac{\pi}{2}-\phi)\sin^2\phi - \int_0^\phi \ln\cos x \; dx\right]\right\rangle \quad (25)$$

There remains now only the task of evaluating the integral of the lncosx. To accomplish this, lncosx is approximated as follows:

$$\ln\cos x \cong \ln\left(\frac{\frac{\pi}{2}-x}{\frac{\pi}{2}}\right) + \frac{2}{\pi}x - \frac{\pi^2-4}{2\pi^2}x^2 \quad (26)$$

This expression was obtained by matching the end point values and the first and second derivatives at $x = 0$, and requiring the limit of the ratio of the two expressions to approach unity as $x \to \pi/2$. Good agreement is shown in the comparison of the two expressions in Fig. 6. Performing the integral yields:

$$\int_0^\phi \ln\cos x \; dx = -\frac{\pi}{2}\left[(1-\frac{2}{\pi}\psi)\ln(1-\frac{2}{\pi}\phi) + \frac{2}{\pi}\phi\right] + \frac{1}{\pi}\phi^2 - \frac{\pi^2-4}{6\pi^2}\phi^3 \quad (27)$$

Combining this result with Eq. (25) yields the final result for $0 < \phi < \pi/2$:

$$\frac{q_b}{q_{b,o}}\left\langle\cos\phi + \frac{48}{\pi(3\pi^2-8)}\left|\frac{\sin\phi}{2}\left[(\frac{\pi}{2}-\phi)\sin^2\phi + \phi\right.\right.\right.$$

$$\left.\left.- \frac{1}{8}\sin 2\phi + \frac{3}{8}(\frac{\pi}{2}\tan^2\phi - \frac{\phi}{\cos^2\phi} - \tan\phi)\right]\right.$$

$$\left.- \frac{\pi}{8}\cos\phi\left[\pi\phi - (\frac{\pi}{2}-\phi)\sin 2\phi - \phi^2 - \frac{1}{2}\sin^2\phi\right.\right.$$

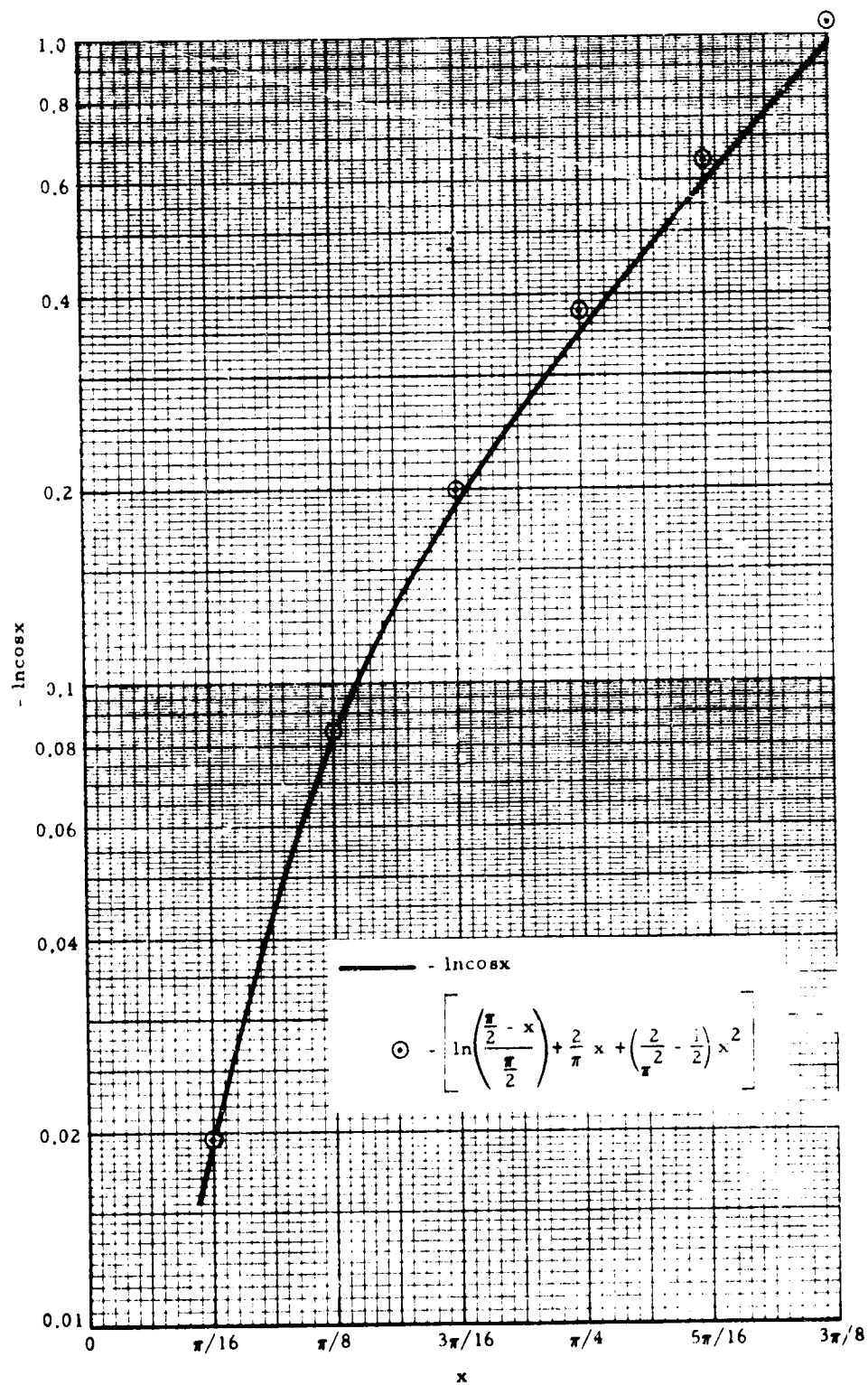Fig. 6 - Comparison of Approximate and Exact Expressions for lncosx

$$+ \frac{1}{2} \tan^2\phi \left((\frac{\pi}{2} - \phi) \tan\phi - 1 \right) \biggr] + (\frac{\pi}{2} - 1) \frac{\cos^2\phi}{\sin\phi} \left[\frac{1}{32} \left(3(\frac{\pi}{2} - \phi) \tan^4\phi - 3 \tan^3\phi + \tan\phi \right. \right.$$

$$\left. + 2 \sin 2\phi - 5\phi \right) - (\frac{\pi}{2} - \phi) \ln\cos\phi - \frac{1}{2} (\frac{\pi}{2} - \phi) \sin^2\phi + \frac{\pi}{2} \left((1 - \frac{2}{\pi}\phi) \ln(1 - \frac{2}{\pi}\phi) + \frac{2}{\pi}\phi \right)$$

$$\left. \left. - \frac{1}{\pi} \phi^2 + \frac{\pi^2 - 4}{6\pi^2} \phi^3 \right] \right] \right\rangle \tag{28}$$

For $\pi/2 < \phi < \pi$, Eq. (7) becomes

$$\frac{q_b}{q_w} = \frac{1}{\sqrt{2\pi}} \frac{S_b}{Kn} \frac{\sigma_{e-\infty}}{\sigma_\infty}$$

$$\times \left\{ -\cos\psi \int_{\pi/2-\psi}^{\pi/2} \cos^{-1} \frac{1}{\tan\psi \tan\phi'} \cos^2\phi' \left(\phi' + \frac{3}{8} \frac{\phi'}{\sin^4\phi'} - \frac{1}{4} \frac{\cos\phi'}{\sin\phi'} - \frac{3}{8} \frac{\cos\phi'}{\sin^3\phi'} \right) d\phi' \right.$$

$$\left. + \cos\psi \int_{\pi/2-\psi}^{\pi/2} \sqrt{\tan^2\psi \tan\phi' - 1} \cos^2\phi' \left(\phi' + \frac{3}{8} \frac{\phi'}{\sin^4\phi'} - \frac{1}{4} \frac{\cos\phi'}{\sin\phi'} - \frac{3}{8} \frac{\cos\phi'}{\sin^3\phi'} \right) d\phi' \right\} \tag{29}$$

where $\psi = \pi - \phi$. Comparing Eq. (29) to Eq. (20) reveals the two equations to
be identical except for the absence in Eq. (29) of the first integral in Eq. (20),
and the substitution of $\pi - \phi$ for ϕ. The results obtained for $0 < \phi < \pi/2$ can
be used, therefore, to obtain results for $\pi/2 < \phi < \pi$:

$$\frac{q_{b,\phi}}{q_{b,o}} = \frac{q_{b,\pi-\phi}}{q_{b,o}} - \cos(\pi - \phi) \tag{30}$$

Note that the results for $\phi > \pi/2$ ignore the absence of scattering in
the "shadowed" volume behind the sphere. This is of no real consequence,

2-16

however, since, as is shown in the following paragraph, the calculated back-scatter flux rapidly decreases as ϕ increases beyond $\pi/2$.

The variation in backscatter flux with ϕ, as determined from Eqs. (17), (28) and (30), is given in tabular form in Table 1, and graphically in Fig. 7.

Table 1

VARIATION OF BACKSCATTER FLUX WITH ANGULAR DISPLACEMENT
ON SPHERE (INTERACTION WITH AMBIENT ATMOSPHERE ONLY)

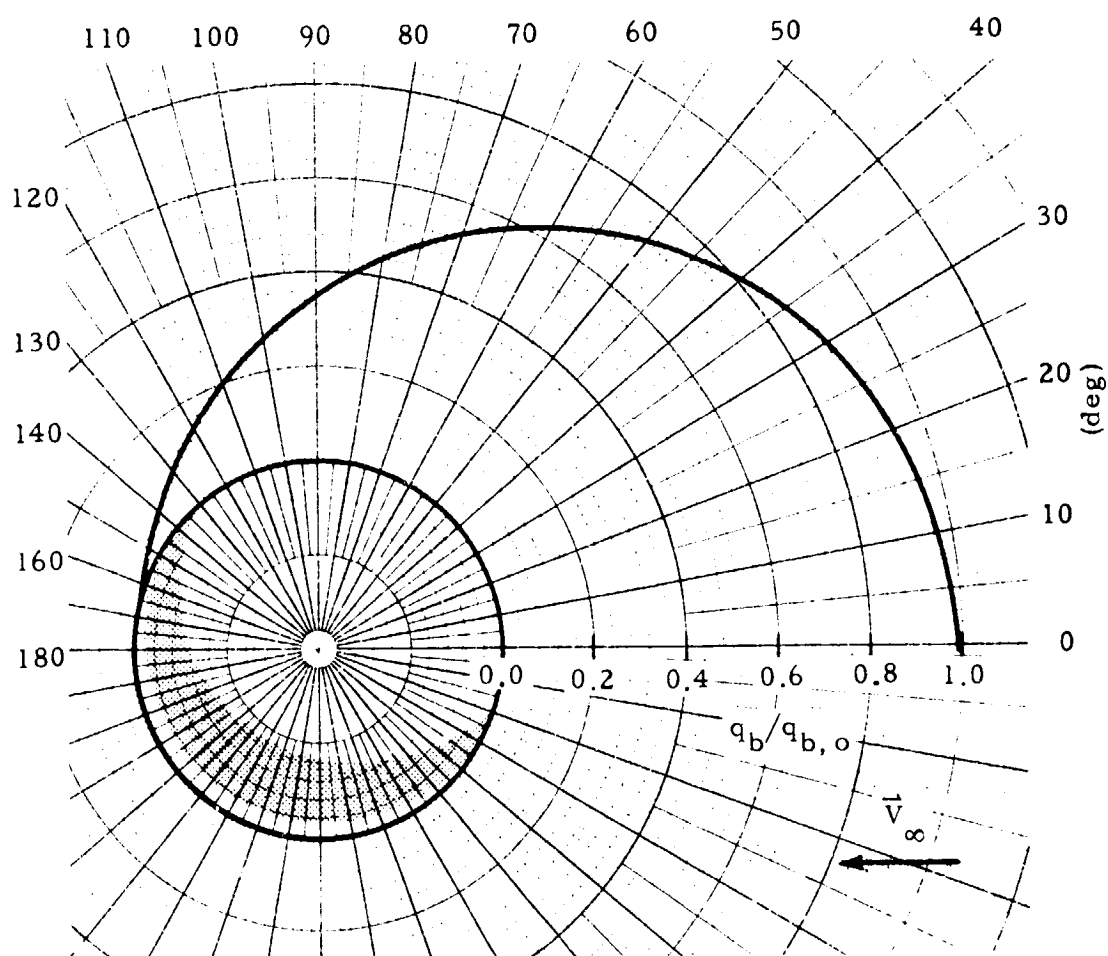| ϕ (deg)	$q_b/q_{b,o}$	ϕ (deg)	$q_b/q_{b,o}$
5	.9963	95	.3049
10	.9857	100	.2655
15	.9689	105	.2287
20	.9466	110	.1945
25	.9193	115	.1630
30	.8877	120	.1342
35	.8522	125	.1081
40	.8134	130	.0849
45	.7717	135	.0646
50	.7276	140	.0474
55	.6816	145	.0331
60	.6341	150	.0217
65	.5856	155	.0130
70	.5365	160	.0070
75	.4875	165	.0030
80	.4391	170	.0009
85	.3920	175	.0002
90	.3471	180	— 0 —

Fig. 7 - Variation of Backscatter Flux with Angular Displacement on Sphere
(Interaction with Ambient Atmosphere Only)

2.2.3   Scattering Due to Collisions Between Outflow Molecules

It will be assumed for the moment that the contribution to the backscatter flux due to collisions between individual outflow molecules is small compared to that due to collisions with ambient atmospheric molecules. This assumption will be shown later to be essentially true when outgassing alone is considered. The truth of this assumption justifies the use of certain simplifying assumptions in the derivation of the backflow due to self-scattering which would otherwise be considered somewhat extreme. The assumptions will produce conservative results in that the calculated values will be greater than would be the case without the assumptions. In addition to the usual first-collision assumptions, it is assumed that the outflow molecules contained in an element of volume are composed of two groups, with the two groups traveling in opposite directions at their mean thermal velocity. The collision rate per unit volume is determined from the collisions between these two groups. In addition, it is assumed that the scattered molecules resulting from these collisions flow outward from the volume element with a spherically symmetrical directional distribution.

Based on the above assumptions, the collision rate $\dot{n}$ per unit volume is given by:

$$\dot{n} = \frac{n_e}{2} \cdot \frac{n_e}{2} \cdot (2\,\overline{v}_w)\,\sigma_{e-e} \tag{31}$$

where σ_{e-e} is the cross section for collisions between outflowing molecules. Making use of Eqs. (3) and (10) yields:

$$\dot{n} = \frac{2\,q_w^2\,\sigma_{e-e}}{\overline{v}_w}\left(\frac{R^2}{r^2} + \frac{R^6}{r^6}\right)^2 \tag{32}$$

Now, referring again to Fig. 3, the flux dq_b of backscattered molecules from collisions in volume element dV at P and crossing surface element dA at Q is

$$dq_b = \frac{\dot{n}\,\cos\beta}{4\pi\,r'^2} \tag{33}$$

2-19

Using Eq. (32) and integrating over the entire half-space outward from dA at a point Q on the sphere surface (refer again to Fig. 1) yields:

$$\frac{q_b}{q_w} = \frac{q_w \, \sigma_{e-e} \, R}{\overline{v}_w} \int_0^{\pi/2} \sin\phi' \, \cos\phi' \left\{ \int_0^\infty \frac{d\widetilde{r}'}{\left(1 + 2\cos\phi' \, \widetilde{r}' + \widetilde{r}'^2\right)^2} \right.$$

$$\left. + 2\int_0^\infty \frac{d\widetilde{r}'}{\left(1 + 2\cos\phi' \, \widetilde{r}' + \widetilde{r}'^2\right)^4} + \int_0^\infty \frac{d\widetilde{r}'}{\left(1 + 2\cos\phi' \, \widetilde{r}' + \widetilde{r}'^2\right)^6} \right\} d\phi' \qquad (34)$$

The grouping of parameters preceding the integral sign in Eq. (34) may be considered an inverse Knudsen number characteristic of self-scattering:

$$\frac{q_w \, \sigma_{e-e} \, R}{\overline{v}_w} = Kn_{e-e}^{-1} \qquad (35)$$

The integrals over $\widetilde{r}'$ in Eq. (34) are as follows:

$$\int_0^\infty \frac{d\widetilde{r}'}{\left(1 + 2\cos\phi' \, \widetilde{r}' + \widetilde{r}'^2\right)^2} = \frac{1}{2} \frac{\phi'}{\sin^3\phi'} - \frac{1}{2} \frac{\cos\phi'}{\sin^2\phi'} \qquad (36)$$

$$\int_0^\infty \frac{d\widetilde{r}'}{\left(1 + 2\cos\phi' \, \widetilde{r}' + \widetilde{r}'^2\right)^4} = \frac{5}{16} \frac{\phi'}{\sin^7\phi'} - \frac{5}{24} \frac{\cos\phi'}{\sin^4\phi'} - \frac{5}{16} \frac{\cos\phi'}{\sin^6\phi'} - \frac{1}{6} \frac{\cos\phi'}{\sin^2\phi'} \qquad (37)$$

$$\int_0^\infty \frac{d\widetilde{r}'}{\left(1 + 2\cos\phi' \, \widetilde{r}' + \widetilde{r}'^2\right)^6} = \frac{63}{256} \frac{\phi'}{\sin^{11}\phi'} - \frac{63}{256} \frac{\cos\phi'}{\sin^8\phi'} - \frac{63}{256} \frac{\cos\phi'}{\sin^{10}\phi'}$$

$$- \frac{21}{160} \frac{\cos\phi'}{\sin^6\phi'} - \frac{9}{80} \frac{\cos\phi'}{\sin^4\phi'} - \frac{1}{10} \frac{\cos\phi'}{\sin^2\phi'} \qquad (38)$$

2-20

Using Eqs. (36) through (38), Eq. (34) now becomes

$$
\begin{aligned}
\frac{q_b}{q_w} = Kn_{e-e}^{-1} \Bigg\{ &\frac{1}{2} \int_0^{\pi/2} \phi' \frac{\cos\phi'}{\sin^2\phi'} d\phi' - \frac{1}{2} \int_0^{\pi/2} \frac{\cos^2\phi'}{\sin\phi'} d\phi' \\
&+ \frac{5}{8} \int_0^{\pi/2} \phi' \frac{\cos\phi'}{\sin^6\phi'} d\phi' - \frac{5}{12} \int_0^{\pi/2} \frac{\cos^2\phi'}{\sin^3\phi'} d\phi' - \frac{5}{8} \int_0^{\pi/2} \frac{\cos^2\phi'}{\sin^5\phi'} d\phi' \\
&- \frac{1}{3} \int_0^{\pi/2} \frac{\cos^2\phi'}{\sin\phi'} d\phi' + \frac{63}{256} \int_0^{\pi/2} \phi' \frac{\cos\phi'}{\sin^{10}\phi'} d\phi' - \frac{63}{384} \int_0^{\pi/2} \frac{\cos^2\phi'}{\sin^7\phi'} d\phi' \\
&- \frac{63}{256} \int_0^{\pi/2} \frac{\cos^2\phi'}{\sin^9\phi'} d\phi' - \frac{21}{160} \int_0^{\pi/2} \frac{\cos^2\phi'}{\sin^5\phi'} d\phi' - \frac{9}{80} \int_0^{\pi/2} \frac{\cos^2\phi'}{\sin^3\phi'} d\phi' \\
&- \frac{1}{10} \int_0^{\pi/2} \frac{\cos^2\phi'}{\sin\phi'} d\phi' \Bigg\}
\end{aligned}
\tag{39}
$$

Carrying out all of the integrals in Eq. (39) would be extremely laborious and, considering the assumptions involved in the derivation of this equation, rather unprofitable. For this reason, only the first term within the brackets in Eq. (34), and, hence, the first two terms in Eq. (39), will be retained in the following development. Carrying out the integration of these terms yields

$$
\frac{q_b}{q_w} = \frac{4-\pi}{4} Kn_{e-e}^{-1}
\tag{40}
$$

2-21

Section 3
APPLICATION TO SKYLAB SPACECRAFT

A typical configuration of the Skylab spacecraft, with the Apollo Telescope Mount (ATM), is shown in Fig. 8. An equivalent size sphere would be roughly 15 to 20 m in diameter. For purposes of this analysis, an equivalent diameter of 20 m (or a radius of 10 m) is assumed.

The operating altitude of the Skylab spacecraft is 435 kilometers. At this altitude, the ambient mean free path is 1.38×10^4 m (Ref. 3), and the circular orbit velocity is 7640 m/sec. The spacecraft surface temperature will vary widely, ranging between about 235 and 380°K, depending upon position in orbit and other parameters. Assuming a surface temperature of 300°K and a molecular weight of 24, the most probable thermal velocity of the outflowing molecules is 456 m/sec. Based on the above data, the ambient Knudsen number, Kn, is 691 and the speed ratio S_b is 16.7.

The collision cross section $\sigma_{e-\infty}$ will vary depending on the relative velocity between the colliding particles. This variance is reflected in the temperature variation of viscosity. For hard sphere molecules, the viscosity is proportional to the square root of temperature and inversely proportional to the cross section (Ref. 4). Conversely, the effective cross section may be considered proportional to the square root of temperature and inversely proportional to viscosity. This is expressed as follows:

$$\frac{\sigma_{e-\infty}}{\sigma^*} = \left(\frac{\overline{T}_{e-\infty}}{T^*}\right)^{-(n-\frac{1}{2})} \tag{41}$$
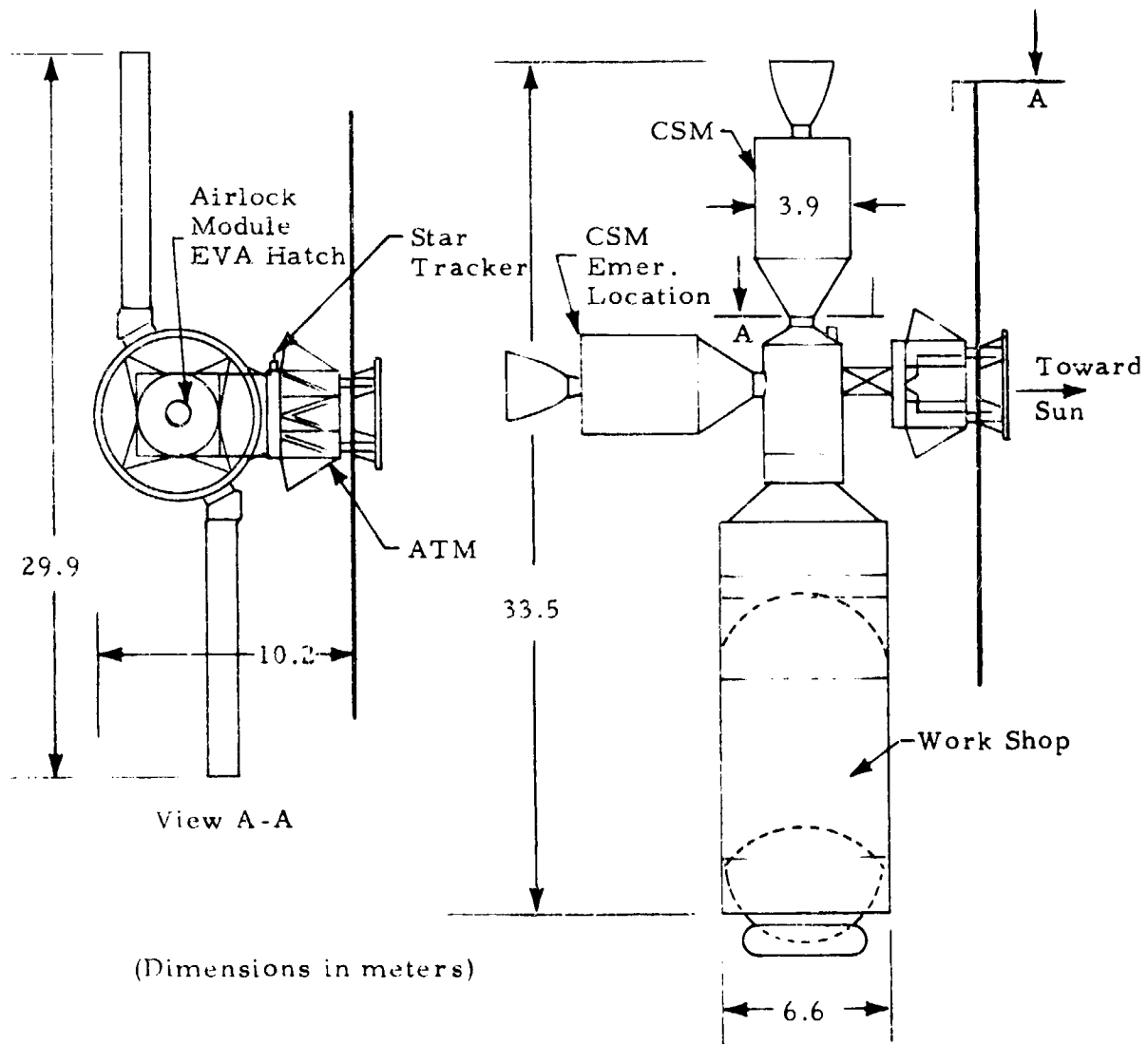
Fig. 8 - Schematic of Typical Configuration of Skylab Spacecraft Showing Approximate External Dimensions

where $\overline{T}_{e-\infty}$ is an effective temperature corresponding to the relative velocity between colliding molecules, σ^* is the cross section at a reference temperature T^*, and n is the exponent in the power-law variation of viscosity with temperature. Based on molecular data in Ref. 4, a value of $43.0 \times 10^{-16} \ cm^2$ for σ^* at temperature $T^* = 300^\circ K$ is assumed, and a value 0.8 for the exponent n. From atmospheric data in Ref. 3, $\sigma_\infty = 41.9 \times 10^{-16} \ cm^2$. The effective temperature $\overline{T}_{e-\infty}$ can be defined in a number of ways, all of which should be based on a proportionality with the square of the relative velocity. We will define it as follows:

$$\overline{T}_{e-\infty} = \frac{1}{3} \frac{\overline{M}}{R_g} V_\infty^2 \tag{42}$$

where $\overline{M}$ is the average molecular weight of the colliding molecules and R_g is the universal gas constant. This expression is based on the mean-square velocity relationship to temperature for a Maxwellian gas. $\overline{T}_{e-\infty}$ is thus found to be $50,200^\circ K$. Based on the above data, the cross section ratio $\sigma_{e-\infty}/\sigma_\infty$ is found to be 0.22.

Using the values which were obtained for Kn, S_b and $\sigma_{e-\infty}/\sigma_\infty$, the dimensionless factor defined by Eq. (12) is found to be 0.00665. This factor may be considered an inverse Knudsen number $Kn_{e-\infty}^{-1} = R/\lambda_{e-\infty}$ characteristic of collisions between outflowing and ambient molecules. The characteristic mean-free-path $\lambda_{e-\infty}$ is seen to be much greater than the sphere radius, thus justifying the assumption of nearly free molecular flow.

Using the above results and Eq. (15), the backscatter flux at $\phi = 0$, due to interaction with the ambient atmosphere, is now found to be 0.003, or 0.3%, of the outgas rate. If the collision cross section had been considered constant and unaffected by the relative velocity, the cross section ratio $\sigma_{e-\infty}/\sigma_\infty = \sigma^*/\sigma_\infty = 1.13$, and the resulting backscatter flux would be 1.5% of the outgas rate.

From Eqs. (35) and (40) it is seen that the fractional intensity of back-flow due to self-scattering is dependent on the outgas rate. First, assume an outgas rate based on an estimated 30 kg/day total weight loss rate for the Skylab spacecraft. Based on the 10 m radius for the equivalent sphere, this amounts to an outgas rate of 2.77×10^{-8} g/cm^2/sec. Recall that this quantity includes waste dumps, attitude control reaction motor firings, etc., in addition to outgassing. This assumed value is actually about three orders of magnitude greater than that which could be expected for simple outgassing.

From Eq. (35), the inverse Knudsen number Kn_{e-e}^{-1} for self-scattering is found to be 1.39. The characteristic mean-free-path, therefore, is about 0.67 of the sphere radius. This mean-free-path value is of marginally satisfactory magnitude for the first-collision assumptions used in the analysis. From Eq. (40), the backscatter flux due to self-scattering is found to be 0.30, or 30%, of the outgas rate. This value is quite large, and, in view of the lumping together of such contributions as waste dumps and reaction motor firings, the question arises as to the validity of the results.

Waste dumps and reaction motor firings occur itermittently and at rather high instantaneous pressures compared to the average, assuming a continuous discharge. The flow regime, therefore, is actually much more nearly continuum than free molecular, and the mass flow returning to the vehicle is more likely due to direct jet impingement than to intermolecular collisions.

A typical outgas rate for spacecraft materials is 3.9×10^{-11} g/cm^2/sec for BBRC "one" paint, air dried (Ref. 5). For this outgas rate, and still assuming M = 24, Kn_{e-e}^{-1} is 2.4×10^{-3}. The mean-free-path is now about 400 times the sphere radius. This is well within the nearly free molecular flow regime. From Eq. (40) the backscatter flux due to self-scattering is found to be 0.0005, or 0.05%, of the outgas rate.

Section 4

CONCLUDING REMARKS

The derivation of equations in this study is fairly rigorous for back-flow due to interaction with the ambient atmosphere. Some rather extreme simplifying assumptions were made, however, for the case of self-scattering. When outgassing alone is considered, the contribution to backflow due to self-scattering is found to be fairly small, about an order of magnitude smaller than that due to interaction with the ambient atmosphere. The rather extreme simplifying assumptions for self-scattering, therefore, are found to be justified.

When all forms of mass flow from the spacecraft, including waste dumps, reaction motor firings, etc., are averaged together into a single continuous out-flow rate, the density of this averaged outflow is sufficiently high that self-scattering is found to far overshadow interactions with the ambient atmosphere. The simplifications made in the analysis of self-scattering, therefore, greatly reduce the accuracy of the calculated backflow. Also, as was pointed out in the preceding section, the primary mode of backflow onto the spacecraft from waste dumps and reaction motor firings is probably direct jet impingement rather than intermolecular collisions.

Considering outgassing alone, only a small fraction, $1\frac{1}{2}\%$ at most, of the outgas products return to the spacecraft as a result of intermolecular collisions. For some outgas products, even this small amount may significantly contaminate sensitive experiment packages. Considering the total outflow (waste dumps, re-action motor firings, etc.), a rather large fraction, about 30%, was estimated to return to the spacecraft. This is certainly a significant quantity; however questions of accuracy of the analysis, and even its applicability to waste dumps and jets, should be considered in evaluating the results.

Section 5

REFERENCES

1. Baker, R. M. L., Jr., and A. F. Charwat, "Transitional Correction to the Drag of a Sphere in Free Molecule Flow," Phys. Fluids, Vol. 1, March-April 1958, p. 73.

2. Willis, D. R., "A Study of Near-Free Molecule Flow," in PROJECT RAND, Aerodynamics of the Upper Atmosphere (compiled by D. J. Masson), R-339, The Rand Corporation, Santa Monica, Calif., 8-10 June 1959.

3. "U. S. Standard Atmosphere, 1962," Superintendent of Documents, U. S. Government Printing Office, Washington, D. C., December 1962.

4. Kennard, E. H., Kinetic Theory of Gases, McGraw-Hill, New York, 1938.

5. Shrodt, J., "ATM Contamination Follow-On Study," Vol. II, TN 67-68, Ball Brothers Research Corporation, Boulder, Colo., 28 October 1967.

APPENDIX B

to LMSC-HREC TR D306352

LOCKHEED MISSILES & SPACE COMPANY INC.

HUNTSVILLE RESEARCH & ENGINEERING CENTER

HUNTSVILLE RESEARCH PARK

4800 BRADFORD DRIVE, HUNTSVILLE, ALABAMA

PARTICLE CLOUD BUILDUP
DUE TO WASTE DUMPING
FROM ORBITING SPACECRAFT

December 1972

Contract NAS8-26554

by
S. J. Robertson

APPROVED:

B. Hobson Shirley, Supervisor
Aerophysics Section

for J. S. Farrior
Resident Director

FOREWORD

This document presents results of an analysis of particle cloud buildup due to waste dumping from orbiting spacecraft, Contract NAS8-26554, performed by Huntsville Research & Engineering Center, Lockheed Missiles & Space Company, Inc., for the National Aeronautics and Space Administration, George C. Marshall Space Flight Center, Alabama. The MSFC technical monitor for the contract is E.E. Klingman, S&E-SSL-PM.

CONTENTS

Section 1
INTRODUCTION AND SUMMARY

The expulsion of liquid wastes from an orbiting spacecraft results in the buildup of a cloud of ice particles which orbit about the central body (earth, moon, etc.) in much the same fashion as the spacecraft from which they were ejected. In fact, the trajectories of these particles may be not far removed from the orbit of the spacecraft, and some particles may even return to the spacecraft where the orbits intersect. There are two primary areas of concern about this cloud. One is the possibility of interference with optical experiments by light scattering and attenuation, and the other is the contamination of the spacecraft by those particles which eventually return to the spacecraft and stick or condense on it.

To provide an indication of the rate of mass flow return to the space-craft, and the mass distribution of the particle cloud, a theoretical analysis was performed for the case of a spherical spacecraft in a circular orbit ejecting mass uniformly in all directions at a constant rate. The expulsion velocity was assumed identical for all particles. It was found that, neglect-ing aerodynamic drag, the rate of return to the Skylab spacecraft is of the order of the outgas rate of a typical spacecraft material. Aerodynamic drag was found to eliminate the possibility of return flow altogether for Skylab. The optical properties of the particle cloud were found to be not substantially more than that predicted for an isotropic source with the same expulsion rate. Some intensification was found in directions along the spacecraft orbit.

Section 2
DERIVATION OF EQUATIONS

2.1 PARTICLE ORBITS

The orbital motion of the ejected particles is determined in the following analysis by utilizing small perturbation theory as outlined in Ref. 1. The particle orbits are derived as perturbations from the circular orbit of the spacecraft. Spherical polar coordinates r, θ and ϕ are used, where r is the radial distance from the center of the spacecraft orbit, θ is the angular displacement in the plane of the spacecraft orbit, and ϕ is the angular displacement away from the spacecraft orbit plane. The coordinate system is illustrated in Fig. 1. Note that ϕ is defined here somewhat differently than is customary with polar coordinates.

The differential equations for the orbits are

$$\ddot{r} - r \cos^2\phi \; \dot{\theta}^2 - r\dot{\phi}^2 + \frac{\mu}{r^2} + \frac{F_D}{m} \frac{\dot{r}}{v} = 0 \tag{1}$$

$$\ddot{\theta} + 2 \frac{\dot{r}\dot{\theta}}{r} - 2 \frac{\dot{\phi}\dot{\theta} \sin\phi}{\cos\phi} + \frac{F_D}{m} \frac{\dot{\theta}}{v} = 0 \tag{2}$$

$$\ddot{\phi} + 2 \frac{\dot{r}}{r} \dot{\phi} + \dot{\theta}^2 \sin\phi \cos\phi + \frac{F_D}{m} \frac{\dot{\phi}}{v} = 0 \tag{3}$$

where $\mu = \gamma M$, with γ the gravitational constant and M the mass of the central body, F_D is the aerodynamic drag force, m is the particle mass and

$$v = (\dot{r}^2 + r^2 \cos^2\phi \; \dot{\theta}^2 + r^2 \dot{\phi}^2)^{1/2}$$
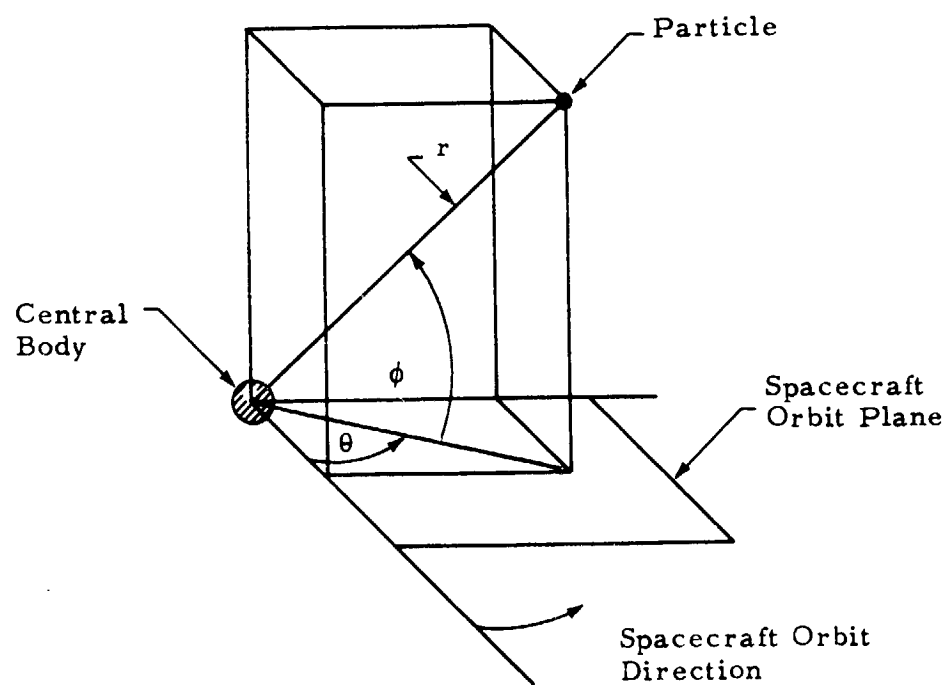
is the instantaneous velocity.

Fig. 1 - Illustration of Coordinate System Used in Orbit Analysis

LOCKHEED - HUNTSVILLE RESEARCH & ENGINEERING CENTER

Taking small perturbations of Eqs. (1) and (2) about the circular spacecraft orbit yields:

$$\ddot{\delta r} + \frac{F_D}{m\, v_o}\, \dot{\delta r} - 3\, \frac{v_o^2}{r_o^2}\, \delta r - 2\, v_o\, \dot{\delta \theta} = 0 \tag{4}$$

$$2\, \frac{v_o}{r_o}\, \dot{\delta r} + r_o\, \ddot{\delta \theta} + \frac{F_D}{m} = 0 \tag{5}$$

where the subscript zero refers to the spacecraft orbit, and δ denotes a perturbation from the spacecraft orbit. Note that v_o and r_o are constant for circular orbits. Equation (3) requires no small perturbation analysis since the angle ϕ is itself a small perturbation from the spacecraft orbit ($\phi_o = 0$).

The solution of the differential equations (Eqs. (3) to (5)) will require that initial values be known at the time of particle expulsion from the space-craft (t = 0). These initial values are listed as follows:

$$\delta r_{t=0} = 0, \quad \dot{\delta \theta}_{t=0} = \frac{v_e \cos \zeta}{r_o}, \quad \dot{\delta r}_{t=0} = v_e\, \sin \zeta\, \cos \eta, \quad \dot{\phi}_{t=0} = \frac{v_e\, \sin \zeta\, \sin \eta}{r_o} \tag{6}$$

where v_e is the expulsion velocity, and ζ and η are spherical polar angles describing the direction of expulsion from the spacecraft. The angles ζ and η are defined in Fig. 2, and the initial values are shown in their relationship to ζ and η.

Equation (5) may be integrated to yield:

$$2\, \frac{v_o}{r_o}\, (\delta r - \delta r_{t=0}) + r_o\, (\dot{\delta \theta} - \dot{\delta \theta}_{t=0}) + \frac{F_D}{m}\, t = 0 \tag{7}$$

With the appropriate initial values, Eq. (7) becomes:

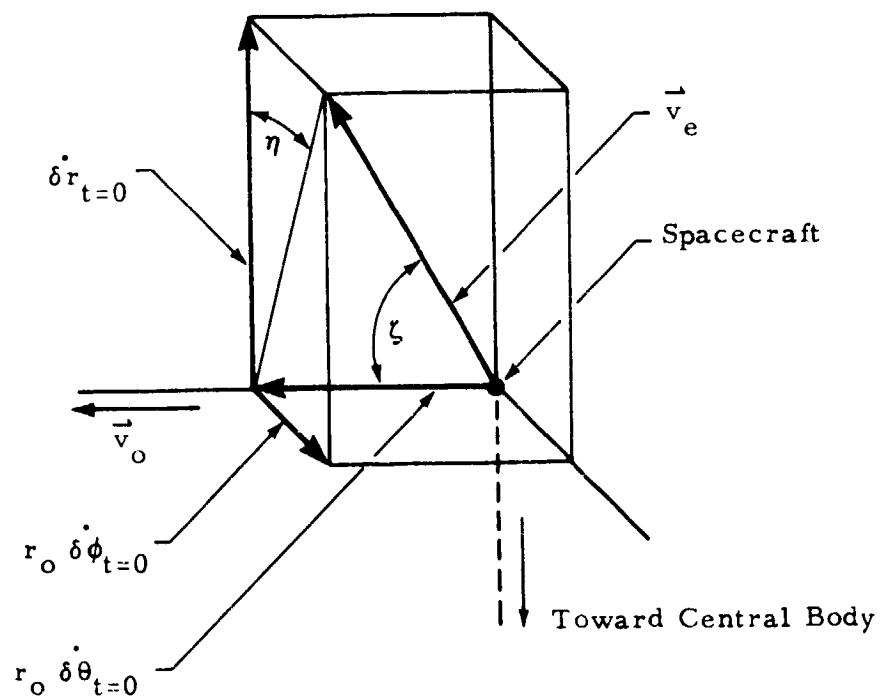$$2\, \frac{v_o}{r_o}\, \delta r + r_o\, \dot{\delta \theta} - v_e\, \cos \zeta + \frac{F_D}{m}\, t = 0 \tag{8}$$

2-3

Fig. 2 - Relationship of Initial Values to Expulsion Direction

LOCKHEED - HUNTSVILLE RESEARCH & ENGINEERING CENTER

Equations (4) and (8) are now combined to eliminate $\delta\dot{\theta}$:

$$\ddot{\delta r} + \frac{F_D}{m v_o} \dot{\delta r} + \frac{v_o^2}{r_o^2} \delta r = 2 \frac{v_o v_e}{r_o} \cos \zeta - 2 \frac{F_D v_o}{m r_o} t \tag{9}$$

Equation (9) is a rather simple linear nonhomogeneous equation with constant coefficients which can be solved with little difficulty. Before finding the solution, however, the order of magnitude of the terms in the equation will be estimated. The following is a list of order of magnitude estimates which we will use in this analysis.

$$\delta r \sim v_e T_o, \quad \dot{\delta r} \sim v_e, \quad \ddot{\delta r} \sim v_e / T_o$$

$$F_D \sim \rho_\infty v_o^2 d_p^2, \quad m \sim \rho_p d_p^3 \tag{10}$$

where ρ_∞ is the atmospheric density at orbit altitude, ρ_p is the mass density of the particle, d_p is the effective particle diameter and $T_o = 2 \pi r_o / v_o$, the spacecraft orbit period.

For the 435 km altitude orbit corresponding to the Skylab spacecraft, ρ_∞ is approximately 3.86×10^{-12} kg/m^3, r_o is 6.8×10^6 m and v_o is 7640 m/sec. The effective particle diameter is estimated from a force balance between surface tension and vapor pressure forces in a water droplet in vacuum.

$$d_p = 4 \tau / p_v \tag{11}$$

2-5

where τ is surface tension and p_v is vapor pressure. For water near the freezing temperature, τ and p_v are approximately 75 dynes/cm and 6660 dynes/cm^2 (5 mm Hg), respectively. The diameter d_p is thus found to be about 0.450 mm.

The expulsion velocity v_e is probably of the order of 10 m/sec, corresponding to a differential pressure of about 7000 kg/m^2 ($\approx$ 10 psi). The particle density ρ_p for water droplets is, of course, 10^3 kg/m^3.

Based on the above results, the order of magnitude of the terms in Eq. (9) are determined and listed as follows:

$$\text{First term} \sim v_e/T_o$$

$$\text{Second term} \sim (\rho_\infty/\rho_p)(r_o/d_p)(v_e/T_o) \sim 10^{-4}(v_e/T_o)$$

$$\text{Third term} \sim v_e/T_o$$

$$\text{Fourth term} \sim v_e/T_o$$

$$\text{Fifth term} \sim \frac{(\rho_\infty/\rho_p)(r_o/d_p)}{(v_e/v_o)} (t/T_o)(v_e/T_o)$$

$$\sim 10^{-1} (t/T_o)(v_e/T_o)$$

The first, third and fourth terms are seen to be of about the same order of magnitude. The second term is clearly negligible compared to the others. The fifth term becomes significant after a few orbit periods and progressively increases in magnitude thereafter. Actually, particle sizes can extend down to the micron range, thus increasing the relative order of magnitude of the second term. Even for a half micron size particle, however, the factor is about 0.1, with the result that the second term may still be safely neglected.

2-6

Neglecting the second term, Eq. (9) is solved to yield:

$$\frac{\delta r}{r_o(v_e/v_o)} = (\sin \zeta \, \cos \eta + \frac{1}{\pi} \frac{F_D T_o}{m \, v_e}) \sin(2\pi t/T_o)$$

$$+ 2 \cos \zeta [1 - \cos(2\pi t/T_o)] - 2 \frac{F_D T_o}{m v_e} (t/T_o) \tag{12}$$

or

$$\delta\tilde{r} = (\sin \zeta \, \cos \eta + \alpha/\pi) \sin(2\pi \tilde{t})$$

$$+ 2 \cos \zeta [1 - \cos(2\pi \tilde{t})] - 2\alpha\tilde{t} \tag{13}$$

where the tilde denotes normalization of δr to the characteristic dimension $r_o (v_e/v_o)$, and t to the orbit period T_o. The aerodynamic drag parameter α is given by

$$\alpha = \frac{F_o T_o}{m \, v_e} \tag{14}$$

Neglecting α, the variation in particle orbit radius from the space-craft orbit is illustrated in Fig. 3. For $\zeta = 0$, the particle orbit is tangent to the spacecraft orbit at the point corresponding to $\tilde{t} = 0, 1, 2 \ldots$. For $\eta = 0$ and $\zeta \neq 0$, the particle orbit crosses the spacecraft orbit at that point and some other point depending on the value of ζ. For $\zeta = \pi/2$, the other point is at $\tilde{t} = 1/2, 3/2, 5/2, \ldots$ For $\eta \neq 0$, the projection of the particle orbit on the spacecraft orbit plane behaves in the same manner as for $\eta = 0$. The effect of α is to continuously decrease the particle orbit radius.
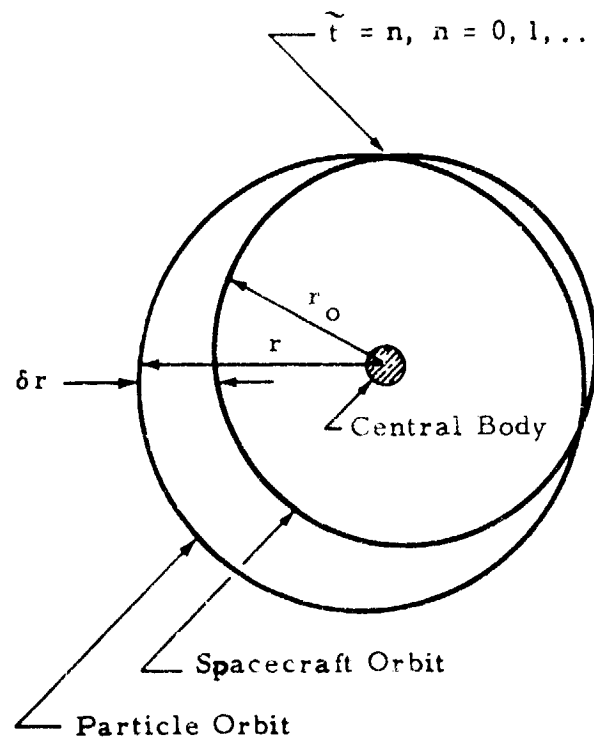
2-7

Fig. 3 - Variation of Particle Orbit Radius from Spacecraft Orbit

Equation (12) may now be combined with Eq. (8) to yield

$$\dot{\delta\theta} = -3\frac{v_e \cos \zeta}{r_o} + 3\frac{F_D t}{mr_o} - 2\frac{v_e}{r_o}(\sin\zeta \cos\eta + \alpha/\pi)\sin(2\pi t/T_o)$$

$$+ 4\frac{v_e}{r_o}\cos \zeta \cos(2\pi t/T_o) \tag{15}$$

which is then integrated and nondimensionalized to yield the final result for the variation of $\delta\theta$:

$$\delta\theta/(v_e/v_o) = -6\pi(\cos \zeta)\tilde{t} + 3\pi\alpha\tilde{t}^2$$

$$- 2(\sin\zeta \cos\eta + \alpha/\pi)\left[1 - \cos(2\pi\tilde{t})\right] + 4\cos \zeta \sin(2\pi\tilde{t})$$

$$\tag{16}$$

Again neglecting α, particles ejected ahead of the spacecraft ($\zeta < \pi/2$) are seen to recede behind the spacecraft, and particles ejected behind the space-craft ($\zeta > \pi/2$) are seen to advance ahead of the spacecraft. Particles ejected normally to the spacecraft trajectory ($\zeta = \pi/2$) and $\eta \neq \pm \pi/2$ are seen to advance and recede over the orbit period, so that $\delta\theta = 0$ at the end of orbit periods. For $\zeta = \pi/2$ and $\eta = \pm \pi/2$, $\delta\theta$ remains constant at zero.

The variation in ϕ is found from the solution of the differential equation, Eq. (3). This equation is nonlinear in form, however, and cannot be readily solved. Before a solution is attempted, the order of magnitude of the terms in the equation will be estimated to determine if the equation can be realistic-ally simplified to a more tractable form. The following is a list of order of magnitude estimates to be used in estimating the order of magnitude of the various terms:

2-9

$$\dot{\phi} \sim \frac{v_e}{r_o}, \quad \ddot{\phi} \sim \frac{v_e}{r_o T_o}, \quad \phi \sim \frac{v_e}{r_o} T_o, \quad \dot{r} \sim v_e \tag{17}$$

Also, the following near-equalities will be assumed:

$$v \cong v_o, \quad r \cong r_o, \quad \dot{\theta} \cong \frac{v_o}{r_o}, \quad \sin\phi \cong \phi, \quad \cos\phi \cong 1 \quad (\phi \ll 1) \tag{18}$$

Using these estimates, the order of magnitude of the terms in Eq. (3) are determined and listed as follows:

$$\text{First term} \sim \frac{v_e}{r_o T_o} \sim \left(\frac{v_e}{v_o}\right) \frac{1}{T_o^2}$$

$$\text{Second term} \sim \left(\frac{v_e}{r_o}\right)^2 \sim \left(\frac{v_e}{v_o}\right)^2 \frac{1}{T_o^2}$$

$$\text{Third term} \sim \left(\frac{v_o}{r_o}\right)^2 \cdot \frac{v_e T_o}{r_o} \sim \left(\frac{v_e}{v_o}\right) \frac{1}{T_o^2}$$

$$\text{Fourth term} \sim \frac{F_D}{m v_o} \frac{v_e}{r_o} \sim \alpha \left(\frac{v_e}{v_o}\right)^2 \frac{1}{T_o^2}$$

The first and third terms are seen to be about the same order of magnitude. The second term differs by the factor v_e/v_o, and the fourth term differs by $\alpha (v_e/v_o)$. Previous results show $v_e/v_o \sim 10^{-3}$ and $\alpha \sim 10^{-1}$. The second and fourth terms, therefore, will be neglected. Taking into account the near-equalities of Eqs. (18) and dropping the second and fourth terms, Eq. (3) becomes:

$$\ddot{\phi} + (v_o/r_o)^2 \phi = 0 \tag{19}$$

With the initial values in Eq. (6), the solution of Eq. (19) becomes:

$$\phi / (v_e / v_o) - \sin \ \zeta \ \sin \eta \ \sin (2 \pi \widetilde{t}) \tag{20}$$

Equation (20) reveals that particles ejected from the spacecraft in a direction out of the spacecraft orbit plane will swing back and forth across the orbit plane, crossing the plane at times corresponding to half and whole values of orbit periods ($t = n/2$, $n = 1, 2, \ldots$).

2.2 RETURN MASS FLOW RATE

Reviewing the results of the preceding section, neglecting α, the particle position was found to coincide with the spacecraft position at the end of whole orbit periods when $\zeta = \pi/2$ and at the end of half orbit periods when both $\zeta = \pi/2$ and $\eta = \pm \pi/2$. Therefore, particles ejected within two small solid angle regions about $\zeta = \pi/2$ and $\eta = \pm \pi/2$ will collide with a finite diameter spacecraft at the end of a half orbit period, and particles ejected within a small range of ζ about $\pi/2$ (for all ζ) will collide with the spacecraft at the end of a whole orbit period. In the following paragraphs, the range of ζ and η for which collisions occur are found, and the resulting return mass flow rate is determined.

The distance d of the particle from the spacecraft is given by (for $d/r_o \ll 1$):

$$d/r_o = \left[(\delta r/r_o)^2 + \delta \theta^2 + \phi^2 \right]^{1/2} \tag{21}$$

By setting d equal to the spacecraft radius R (assumed spherical) at the times of closest approach ($\widetilde{t} = 1/2$ and 1), the limiting range of ζ and η for particle collisions with the spacecraft can be determined.

For $\widetilde{t} = 1/2$, we obtain the following expression:

$$\widetilde{R} = \left| (16 + 9 \pi^2) \cos^2 \zeta + 24 \pi \sin \zeta \cos \zeta \cos \eta \right.$$

2-11

$$+ 16 \sin^2 \zeta \cos^2 \eta - (5 - 9\pi^2/16 - 16/\pi^2) \alpha^2$$

$$+ \left[(16 + 9\pi^2/2) \cos \zeta - (32/\pi - 6\pi) \sin \zeta \cos \eta \right] \alpha \Big\}^{1/2} \tag{22}$$

For the Skylab spacecraft, an effective radius R of about 10 m may be assumed. Using the values of r_o, v_e and v_o given in the preceding section, the left side of Eq. (22) takes on the value 1.12×10^{-3}. This requires that, for Eq. (22) to be satisfied, the square root of each term under the radical be no greater than the order 10^{-3}. Since α is of order 10^{-1} for the Skylab spacecraft, this implies that no particle collisions can occur. Neglecting aerodynamic drag ($\alpha = 0$), we find that $\cos \zeta \sim \cos \eta \sim 10^{-3}$, or $\zeta \cong \pi/2$ and $\eta \cong \pm \pi/2$ in accordance with our previous findings. Equation (22) may now be simplified by changing variables and using appropriate approximations as follows:

$$(16 + 9\pi^2) \Delta_\zeta^2 + 24 \, \Delta_\zeta \, \Delta_\eta + 16 \, \Delta_\zeta^2 = \widetilde{R}^2 \tag{23}$$

where $\Delta_\zeta = \pi/2 - \zeta$ and $\Delta_\eta = \pm \pi/2 - \eta$. Equation (23) is seen to be the equation of very small ellipses about $\zeta = \pi/2$ and $\eta = \pm \pi/2$ on a unit radius sphere. The solid angle enclosed by these ellipses is simply their area. From analytic geometry, the axis of the ellipse is seen to be rotated from the Δ_η axis by an angle θ given by

$$\theta = (1/2) \tan^{-1} (8/3\pi) = 20.17^o \tag{24}$$

and the two semi-axes a and b are given by

$$a = \frac{\widetilde{R}}{\left\{ (16 + 9\pi^2) \cos^2 \theta + 24\pi \sin \theta \cos \theta + 16 \sin^2 \theta \right\}^{1/2}}$$

2-12

$$= 0.0917\widetilde{R} \tag{25}$$

and

$$b = \frac{\widetilde{R}}{\left\{(16 + 9\pi^2)\sin^2\theta - 24\pi\sin\theta\cos\theta + 16\cos^2\theta\right\}^{1/2}}$$

$$= 0.463\,\widetilde{R} \tag{26}$$

The area and, hence, the solid angle ω is

$$\omega = \pi\, a\, b \tag{27}$$

which, for the two ellipses, amounts to a fraction f of the total solid angle given by

$$f = 2\pi\, ab/(4\pi) = (1/2)\, ab$$

$$= 0.0212\,\widetilde{R}^2 \tag{28}$$

Using the value of $\widetilde{R}$ found in a preceding paragraph, this fraction is found to be 2.66×10^{-8}, which is the fraction of mass flowing from the spacecraft which will return a half orbit period later.

For $\widetilde{t} = 1$, the distance expression (Eq. (21)) becomes

$$\widetilde{R} = \left\{36\pi^2\cos^2\zeta + (9\pi^2 + 4)\,\alpha^2 - 36\pi^2\,\alpha\cos\zeta\right\}^{1/2}$$

$$= \left\{(6\pi\cos\zeta - \alpha)^2 + (9\pi^2 + 3)\alpha^2\right\}^{1/2} \tag{29}$$

2-13

As was the case for $\tilde{t} = 1/2$, the expression cannot be satisfied for the aerodynamic drag anticipated for the Skylab orbit, and, hence, no particle collisions are possible. Neglecting aerodynamic drag, we find that $\cos \zeta \sim 10^{-3}$, or $\zeta \cong \pi/2$, again in accordance with our previous findings. With the appropriate simplifications, Eq. (29) yields

$$\Delta_\zeta = \pm \tilde{R}/6\pi \tag{30}$$

The solid angle enclosed by $\pm \Delta_\zeta$ is found by integrating as follows:

$$\omega = 4\pi \int_0^{\Delta_\zeta} \cos\Delta_\zeta \, d\Delta_\zeta = 4\pi \sin\Delta_\zeta \cong 4\pi \Delta_\zeta$$

$$= (2/3) \tilde{R} \tag{31}$$

The fraction f of the total solid angle is

$$f = \tilde{R}/6\pi \tag{32}$$

For the Skylab spacecraft, this fraction is found to be 5.94×10^{-5}, which is greater than the fraction for $\tilde{t} = 1/2$ by a factor of about 2000. Due to the relative insignificance of the return flow for $\tilde{t} = 1/2$ compared to that for $\tilde{t} = 1$, and since this fraction is included within the fraction for $\tilde{t} = 1$ anyway, we will consider only the fraction for $\tilde{t} = 1$ in our analyses for return mass flow rate. The return mass flow rate $\dot{m}_r$ can now be calculated from

$$\dot{m}_r = \tilde{R} \, \dot{m}/6\pi \tag{33}$$

2.3 DENSITY FIELD ANALYSIS

From the particle orbit equations derived in Section 2.1, the density field of particles ejected from the spacecraft over a period of time can be

2-14

determined. The density ρ at a point P and after a time t is found by carrying out the following integration:

$$\rho_{P,t} = \lim_{\delta V \to 0} \frac{1}{\delta V} \int_0^t \int_{4\pi} \dot{m}\, f_{\zeta,\eta,t'}\, d\omega\, dt' \tag{34}$$

where $\dot{m}$ is the rate of mass expulsion from the spacecraft and $f\, d\omega$ is the fraction of this mass which is expelled during time interval dt' within the solid angle $d\omega$ at ζ and η, and which is contained within the volume element δV at point P after a time t'. This expression includes in the density calculation mass that is moving away from the spacecraft for the first time after having been ejected, and mass that may have been trapped within the particle cloud for some time. For two reasons, our primary concern in these calculations is with the latter portion of mass. First, it is easy enough to calculate the density field for the source-like flow of mass moving away from the spacecraft for the first time. Second, the singular nature of the density field near the source renders any numerical calculations meaningless where large volume elements are used. It will be shown later that, for light scattering purposes, the bulk of the density field of an isotropic source lies within a few source radii. For these reasons, we will not include in the numerical calculations that portion of mass in the source-like flow period of time. For a complete density field calculation, the source-flow density, which can be easily calculated by other means, can be added to the trapped particle density calculations. Since the point at which the source-like flow may be considered terminated is somewhat arbitrary, we will choose a period of time in orbit of 0.3 of an orbit period $(\tilde{t} = 0.3)$ at which to begin our calculations. From Eq. (25), particles ejected out-of-plane reach the maximum out-of-plane displacement at $\tilde{t} = 0.25$.

From Eqs. (13), (16) and (20) the maximum range of a particle in its orbit (neglecting orbit decay) is given by:

$$\left(\frac{\delta r}{r_0}\right)_{max} = \pm\, 4\, \frac{v_e}{v_0} \tag{35}$$

2-15

$$\delta\theta_{max} = \pm\, 6\pi\, \frac{v_e}{v_o}\, \widetilde{t}_{max} \tag{36}$$

$$\phi_{max} = \pm\frac{v_e}{v_o} \tag{37}$$

where $\widetilde{t}_{max}$ is the maximum number of orbit periods under consideration.
The δr and ϕ ranges are divided into 2N equal increments and the $\delta\theta$ range
into $2N\,\widetilde{t}_{max}$ increments to form volume elements of size:

$$\Delta V = \left(\frac{8\,\frac{v_e}{v_o}\,r_o}{2N}\right)\left(\frac{12\pi\,\frac{v_e}{v_o}\,\widetilde{t}_{max}\,r_o}{2N\,\widetilde{t}_{max}}\right)\left(\frac{2\,\frac{v_e}{v_o}\,r_o}{2N}\right) = 24\pi\left[\frac{(v_e/v_o)\,r_o}{N}\right]^3 \tag{38}$$

The number of $\delta\theta$ increments is made proportional to the number of orbits
$\widetilde{t}_{max}$ because the orbit range is proportional to $\widetilde{t}_{max}$. This keeps the volume
element size the same regardless of the number of orbit periods to be con-
sidered.

Next, the total solid angle (4π steradians) about the spacecraft is
divided into nearly equal elements. This is accomplished by first dividing
the ζ range from 0 to π into 2M equal increments $\Delta\zeta$. Then, depending on
the $\Delta\zeta$ increment, the η range from 0 to 2π is divided into the appropriate
number of increments such that the solid angle element $\Delta\omega$ enclosed by $\Delta\zeta$
and $\Delta\eta$ is about the same for each $\Delta\zeta$ increment. This is illustrated in Fig. 4.
The solid angle element $\Delta\omega_o$ between $\zeta = 0$ and $\zeta = \Delta\zeta$ is

$$\Delta\omega_o = 2\pi\,(1 - \cos\Delta\zeta) \tag{39}$$

This conical-shaped element is not further divided into increments of η but
is taken as the basis for dividing the η range for the other elements. The
fraction $\mathscr{F}_o$ of the total solid angle included in $\Delta\omega_o$ is
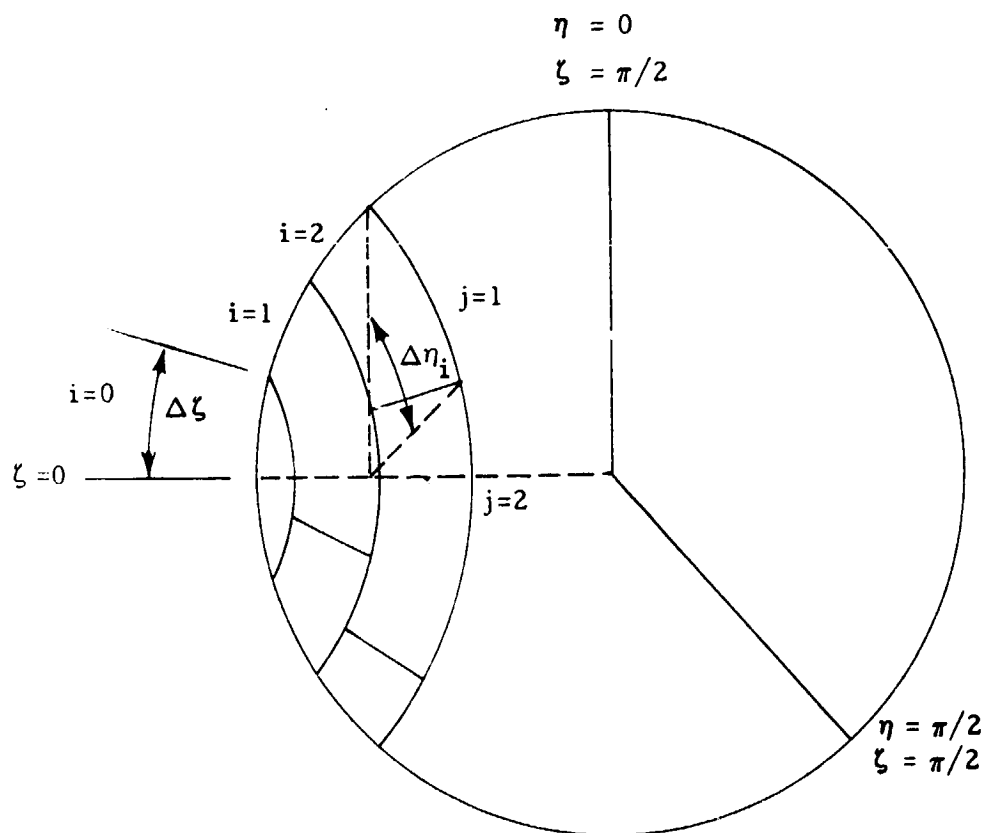
Fig. 4 - Division of Total Solid Angle about Spacecraft into
Approximately Equal Size Elements

$$\mathscr{F}_o = \frac{\Delta\omega_o}{4\pi} = \frac{1}{2}(1 - \cos\Delta\zeta) \tag{40}$$

The solid angle $\Delta\Omega_i$ included between $\zeta = i\,\Delta\zeta$ and $\zeta = (i+1)\,\Delta\zeta$ is

$$\Delta\Omega_i = 2\pi\left\{\cos(i\,\Delta\zeta) - \cos\left[(i+1)\Delta\zeta\right]\right\} \tag{41}$$

This element is further divided into M_{η_i} equal increments of η such that the resulting elements $\Delta\omega_i$ are about the same size as $\Delta\omega_o$. Dividing $\Delta\Omega_i$ by M_{η_i} and equating to $\Delta\omega_o$ yields to the nearest integer:

$$M_{\eta_i} = \text{Integer}\left\{\frac{\cos(i\,\Delta\zeta) - \cos\left[(i+1)\,\Delta\zeta\right]}{1 - \cos\Delta\zeta}\right\} \tag{42}$$

For most practical values of $\Delta\zeta$, M_{η_i} values are found to increase with i in the sequence $3, 5, 7, \ldots$ for the first few values of i. The fraction $\mathscr{F}_i$ of the total solid angle included in $\Delta\omega_i$ is

$$\mathscr{F}_i = \frac{\Delta\omega_i}{4\pi} = \frac{\cos(i\,\Delta\zeta) - \cos\left[(i+1)\,\Delta\zeta\right]}{2\,M_{\eta_i}}. \tag{43}$$

Recall that these values of $\mathscr{F}_i$ should be close to $\mathscr{F}_o$.

Finally, using Eqs. (13), (16) and (20), an amount of mass equal to $\dot{m}\Delta t\,\mathscr{F}_i$ is considered to be ejected from the spacecraft at an instant of time, and a determination is made as to the volume element in which the mass of particles is contained at later times. This is equivalent to solving Eq. (34) in the following fashion:

$$\rho_{i'j'k'N_t} = \frac{\dot{m}\,\Delta t}{\Delta V}\sum_{n_t=1}^{N_t}\sum_{i=1}^{2M}\sum_{j=1}^{M_{\eta_i}}\mathscr{F}_i\,C_{i\,j\,i'\,j'\,k'\,n_t} \tag{44}$$

2-18

where i and j refer to the ζ and η increments, respectively; i', j' and k' refer to the volume element corresponding to the δr, $\delta\theta$ and ϕ increments, respectively; n_t refers to the time step; and $C_{i j i' j' k' n_t} = 1$ or 0 depending on whether the mass of particles from the ij solid angle element is or is not, respectively, in the $i' j' k'$ volume element after a time interval $n_t \Delta t + 0.3 T_o$. (Recall that the time steps begin at $\tilde{t} = 0.3$.) Including the expression for ΔV from Eq. (38), and normalizing Δt to the orbit period T_o, yields:

$$\rho_{i' j' k' N_t} = \frac{\dot{m} T_o \Delta\tilde{t}}{24\pi \left[\frac{(v_e/v_o) r_o}{N}\right]^3} \sum \sum \sum \cdots \tag{45}$$

For convenience, we normalize the local density to an average density $\bar{\rho}$ for mass ejected during a single orbit period and over the maximum range of particles during a single orbit period.

$$\bar{\rho} = \frac{\dot{m} T_o}{\left(8 \frac{v_e}{v_o} r_o\right) \left(12\pi \frac{v_e}{v_o} r_o\right) \left(2 \frac{v_e}{v_o} r_o\right)} = \frac{\dot{m} T_o}{192\pi \left(\frac{v_e}{v_o} r_o\right)^3} . \tag{46}$$

The final result for the normalized density expression is now

$$\tilde{\rho}_{i' j' k' N_t} = \frac{\rho_{i' j' k' N_t}}{\bar{\rho}} = 8 N^3 \Delta\tilde{t} \sum_{n_t=1}^{N_t} \sum_{i=1}^{2M} \sum_{j=1}^{M\eta_i} \mathcal{F}_i C_{i j i' j' k' n_t} \tag{47}$$

A computation procedure based on Eq. (47) was programmed for the NASA-MSFC Univac 1108 digital computer system. A listing of this program is given in the Appendix.

2.4 COLUMN DENSITIES

The parameter of interest in light scattering by the particle cloud is the column density along a line of sight. This parameter is determined as follows:

$$N_c = \int_\Gamma \rho(s)\, ds \qquad (48)$$

where N_c is the column density and the integration is taken along the line of sight Γ. In the present study, the line of sight will originate at the spacecraft and extend out in some direction of interest beyond the outer extent of the particle cloud. We will compare the calculated column densities for the particle cloud with a theoretical column density N_c' for an isotropic spherical source of radius R. This theoretical column density is given by

$$N_c' = \int_R^\infty \frac{\dot{m}}{4\pi\, r^2\, v_e}\, dr = \frac{\dot{m}}{4\pi\, R\, v_e} \qquad (49)$$

where r is the radial distance out from the center of the source. Note from Eq. (49) that the value of the integrand continuously decreases and approaches zero as r increases. There should be some characteristic distance R' out from the source, therefore, within which is contained the bulk of the integral value. By integrating out to the limit R' and requiring the integral value to be some fraction, say 0.9, of the total integral, we determine that 90% of the column density value for an isotropic source is contained within a distance of 10 source radii.

Normalizing the column density N_c in Eq. (48) to the isotropic source column density N_c' in Eq. (49), and normalizing the source radius R and the distance s along the line of sight to the characteristic length $(v_e/v_o)r_o$ for the particle cloud, we change Eq. (48) to the following form:

$$\tilde{N}_c = \frac{\pi}{24} \tilde{R} \int_\Gamma \tilde{\rho}(\tilde{s})\, d\tilde{s} \qquad (50)$$

where the tilde denotes normalized values. Equation (50) may be integrated numerically along a line of sight originating at the spacecraft location and

2-20

extending in any direction. The computer program listed in the appendix performs the integration in six different directions, i.e., in the positive and negative r, θ and ϕ directions away from the spacecraft. The integration procedure uses the trapezoidal formula with the step sizes identical to that used in forming volume elements for the density field analysis.

Section 3

RESULTS

3.1 RETURN MASS FLOW RATE

The return mass flow rate to the Skylab spacecraft was estimated based on the parameters determined in Section 2.2 and on an estimated total weight loss rate of 30 kg/day. Neglecting aerodynamic drag, the return mass flow rate is determined from Eq. (33) to be approximately 2×10^{-8} kg/sec. (Recall that the predicted effect of aerodynamic drag is to prevent mass return to the Skylab.) Based on the 10 m effective radius, this is equivalent to a flux of about 0.7×10^{-11} g/cm^2/sec. A typical outgas rate for spacecraft materials is 4×10^{-11} g/cm^2/sec for BBRC "one" paint, air-dried (Ref. 2). The predicted return mass flow rate is seen to be of the same order of magnitude as this outgas rate.

3.2 PARTICLE CLOUD DENSITY FIELD

The computer program based on Eq. (47) was used to calculate the normalized particle density field about an orbiting spacecraft for durations in orbit up to 10 orbit periods. The dimensionless character of the results makes them applicable to arbitrary conditions of mass expulsion rate and orbital parameters. Calculations were made for zero aerodynamic drag and for drag conditions corresponding to that anticipated for water droplets expelled from the Skylab spacecraft. A particle orbit decay parameter α value of 0.461 was used where drag was considered. Equation (14) was used to calculate α, with the drag force F_D calculated using a drag force coefficient C_D of 2.2, and with the particle diameter, atmospheric density, etc., the same as those used in Section 2.

Results of the density field calculations are shown in Figs. 5 through 12 for a time in orbit up to 10 orbit periods. The position coordinates are appropriately normalized for arbitrary applicability to various expulsion velocities
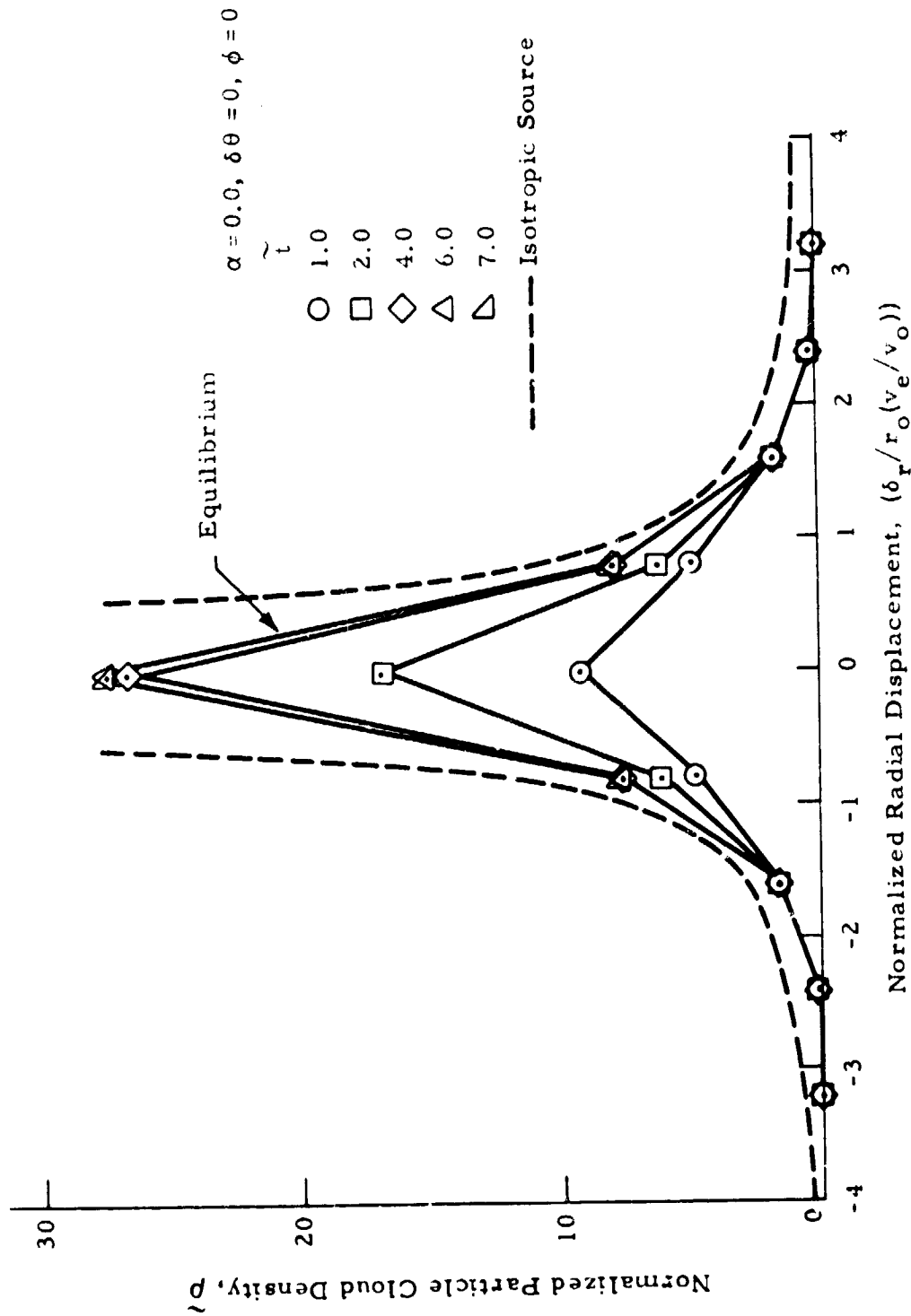
3-1

Fig. 5 - Particle Cloud Density Distribution in Radial Direction as a Function of Time in Orbit (Aerodynamic Drag Neglected)
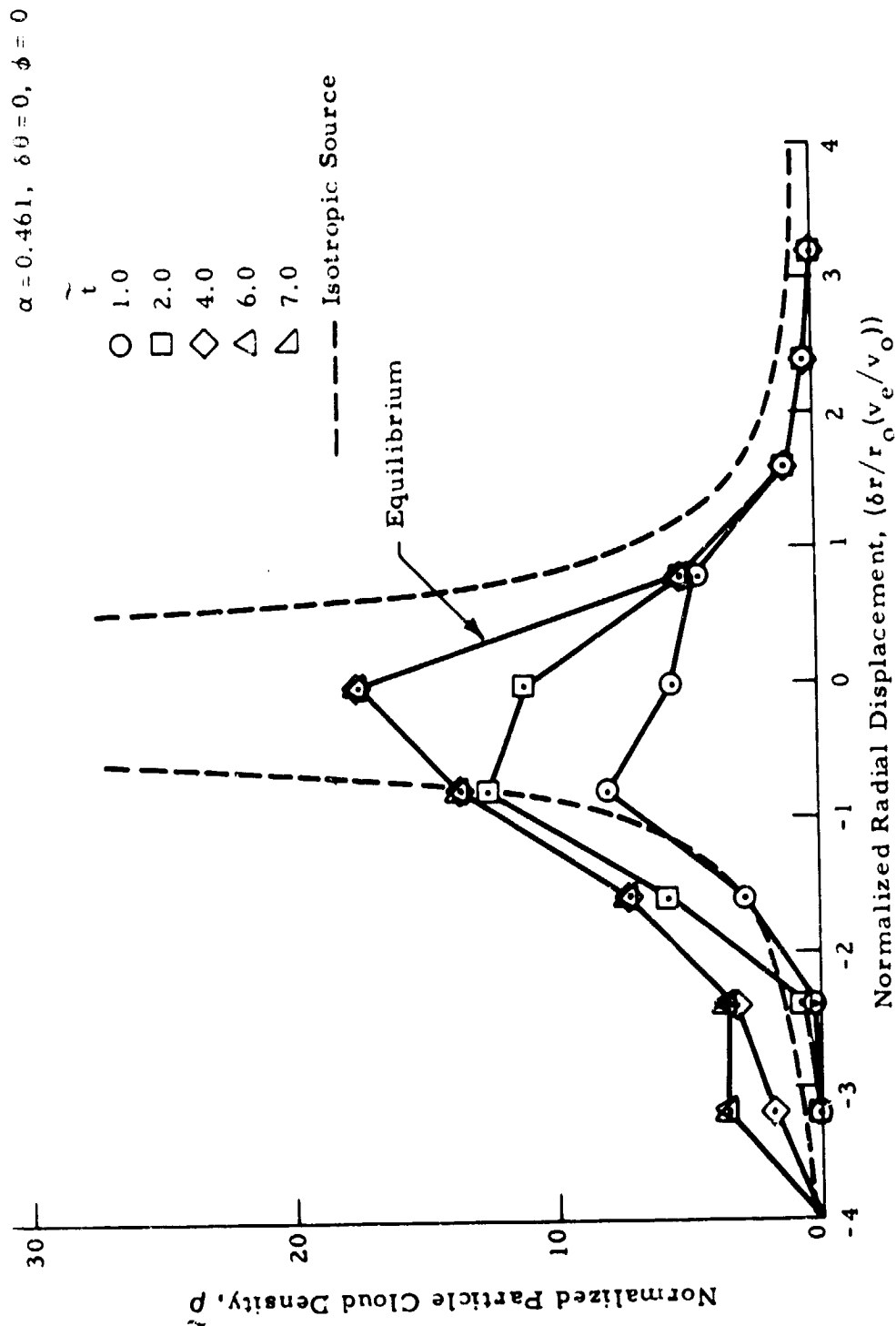
Fig. 6 - Particle Cloud Density Distribution in Radial Direction as a Function of Time in Orbit (Aerodynamic Drag Included)

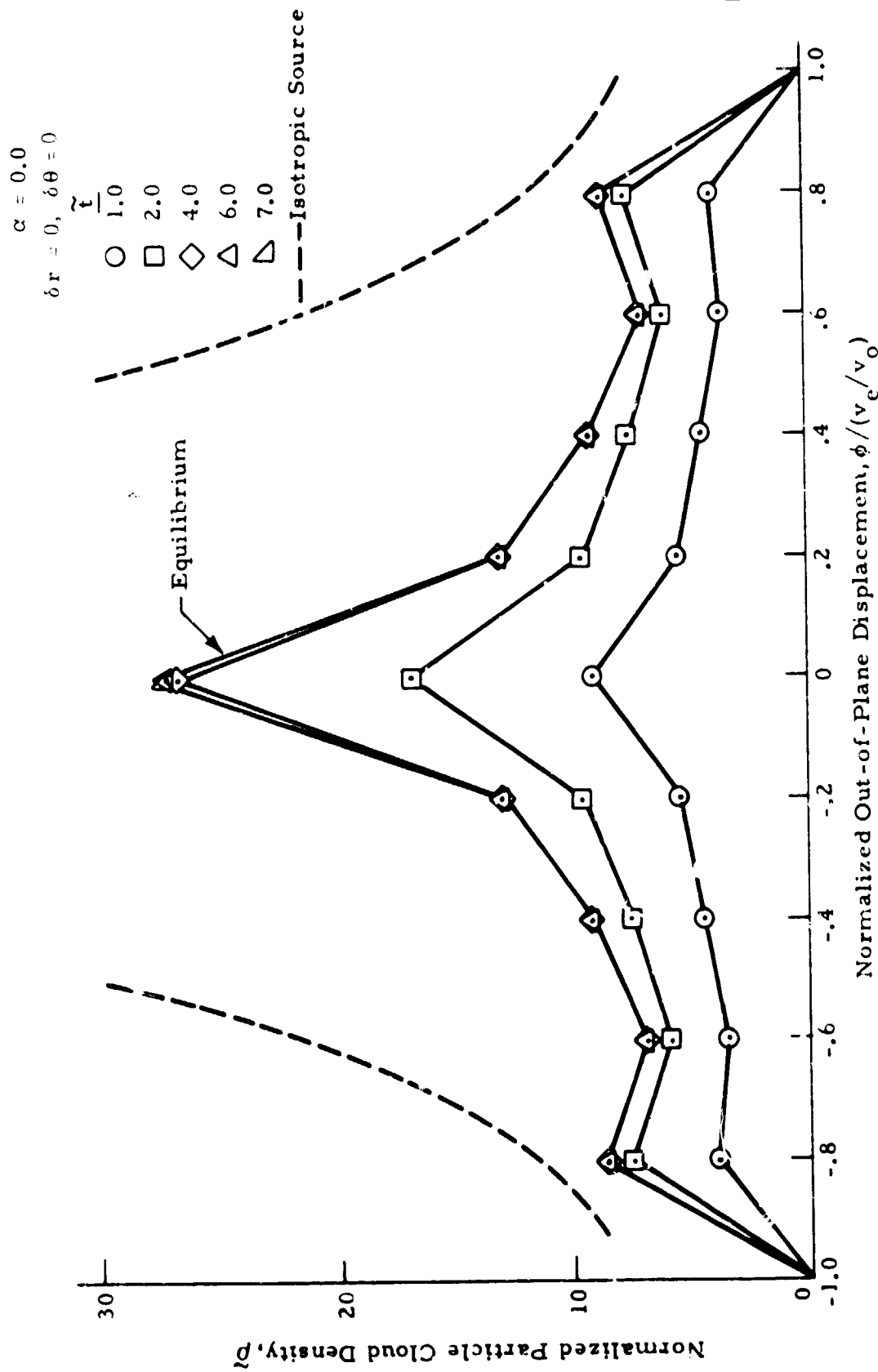Fig. 7 - Particle Cloud Density Distribution in Out-of-Plane Direction as a Function of Time in Orbit (Aerodynamic Drag Neglected)

Fig. 8 - Particle Cloud Density Distribution in Out-of-Plane Direction as a Function of Time in Orbit (Aerodynamic Drag Included)

Fig. 9 – Particle Cloud Density Distribution in In-Plane Angular Direction as a Function of Time in Orbit (Aerodynamic Drag Neglected)
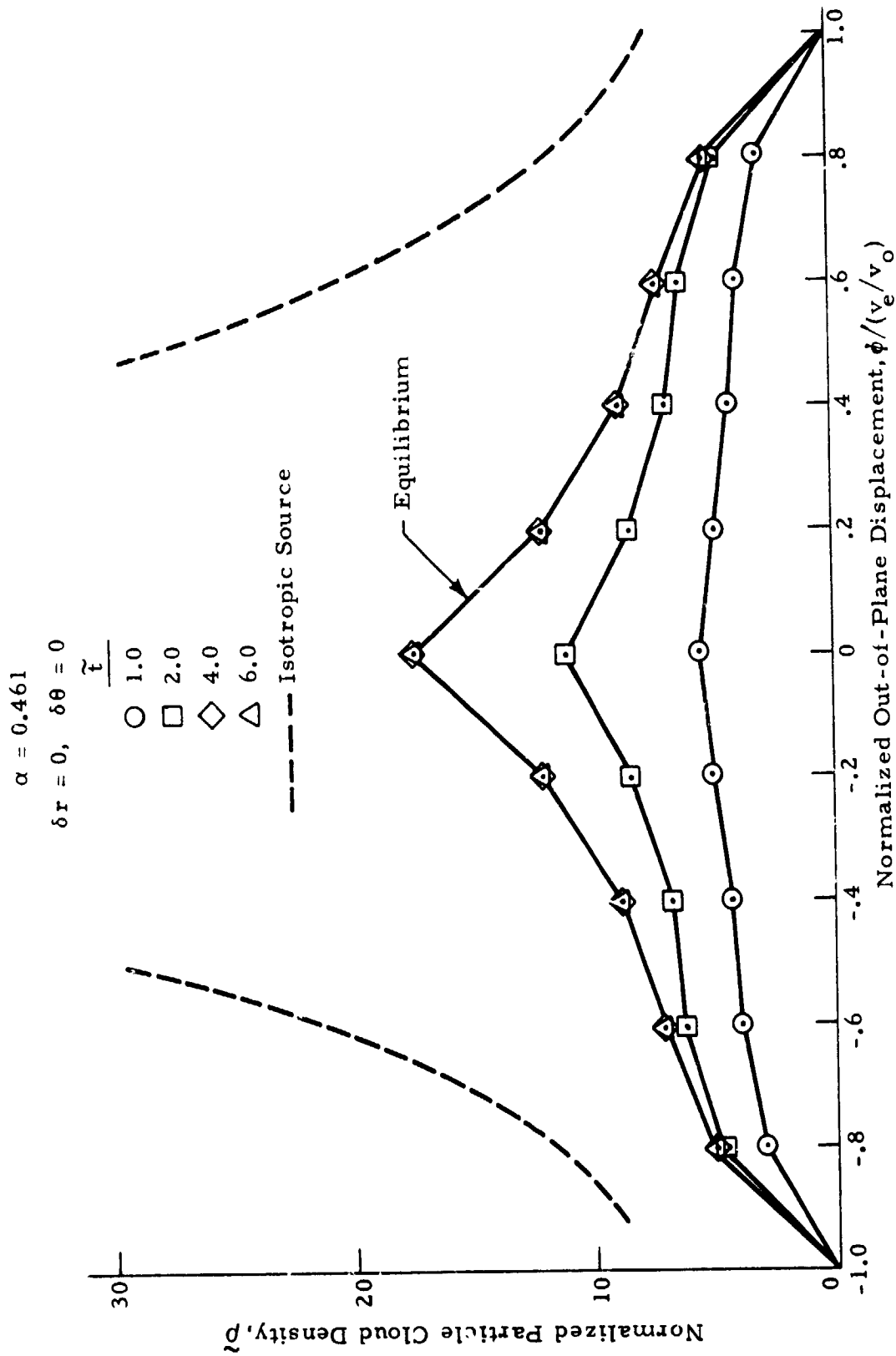
$\alpha = 0.461$

$\delta r = 0, \phi = 0$

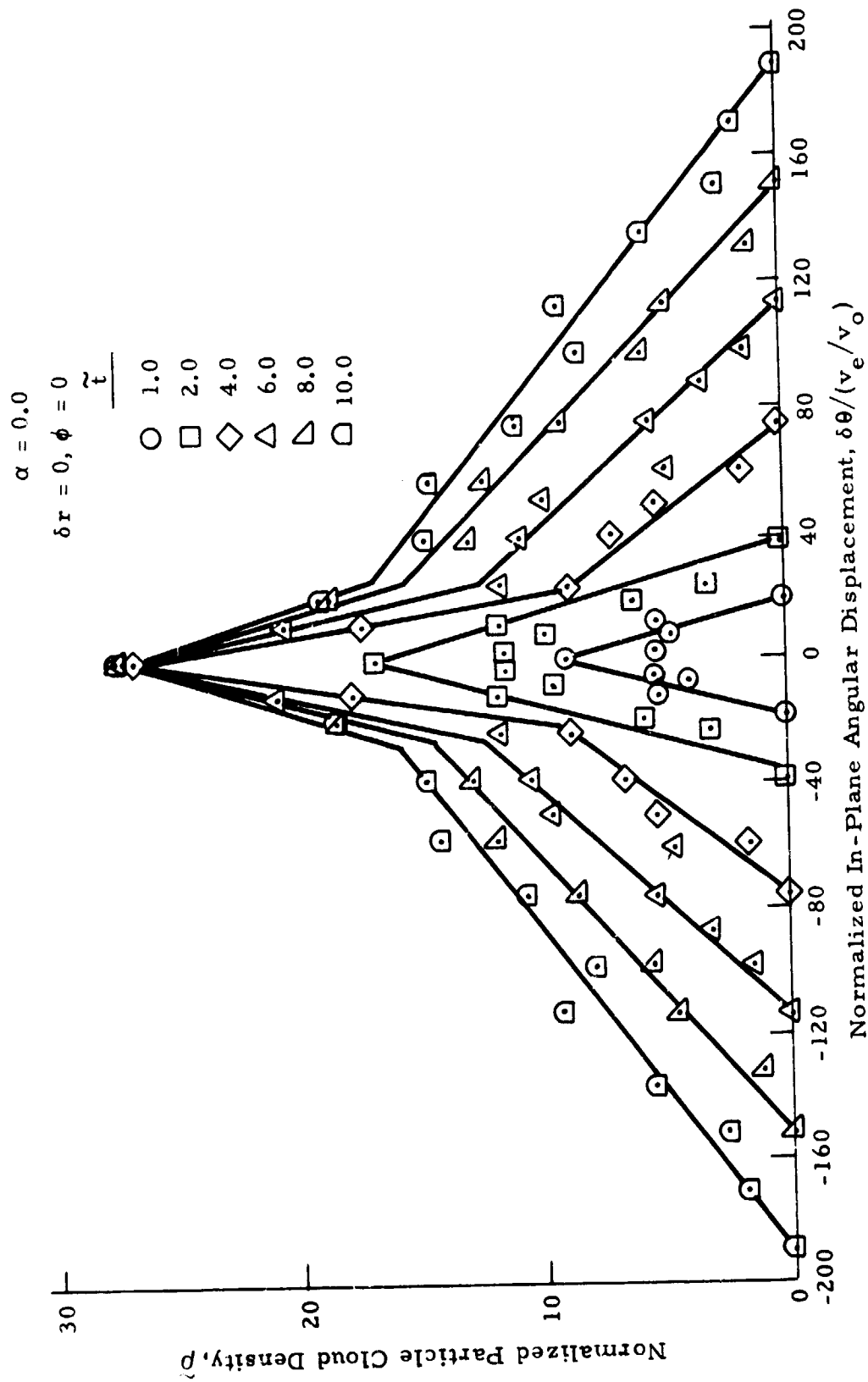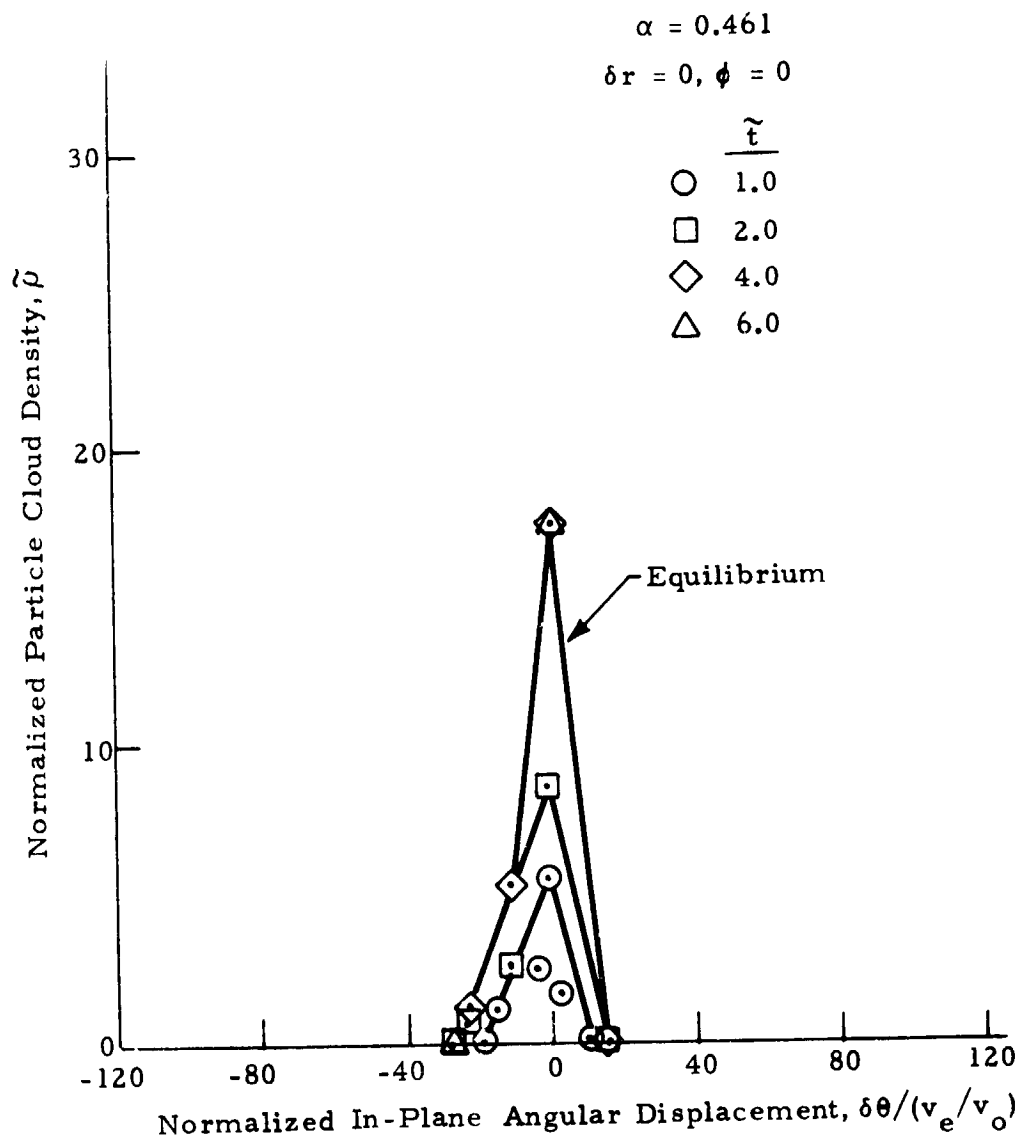Fig. 10 - Particle Cloud Density Distribution in In-Plane Angular
Direction as a Function of Time in Orbit (Aerodynamic
Drag Included)

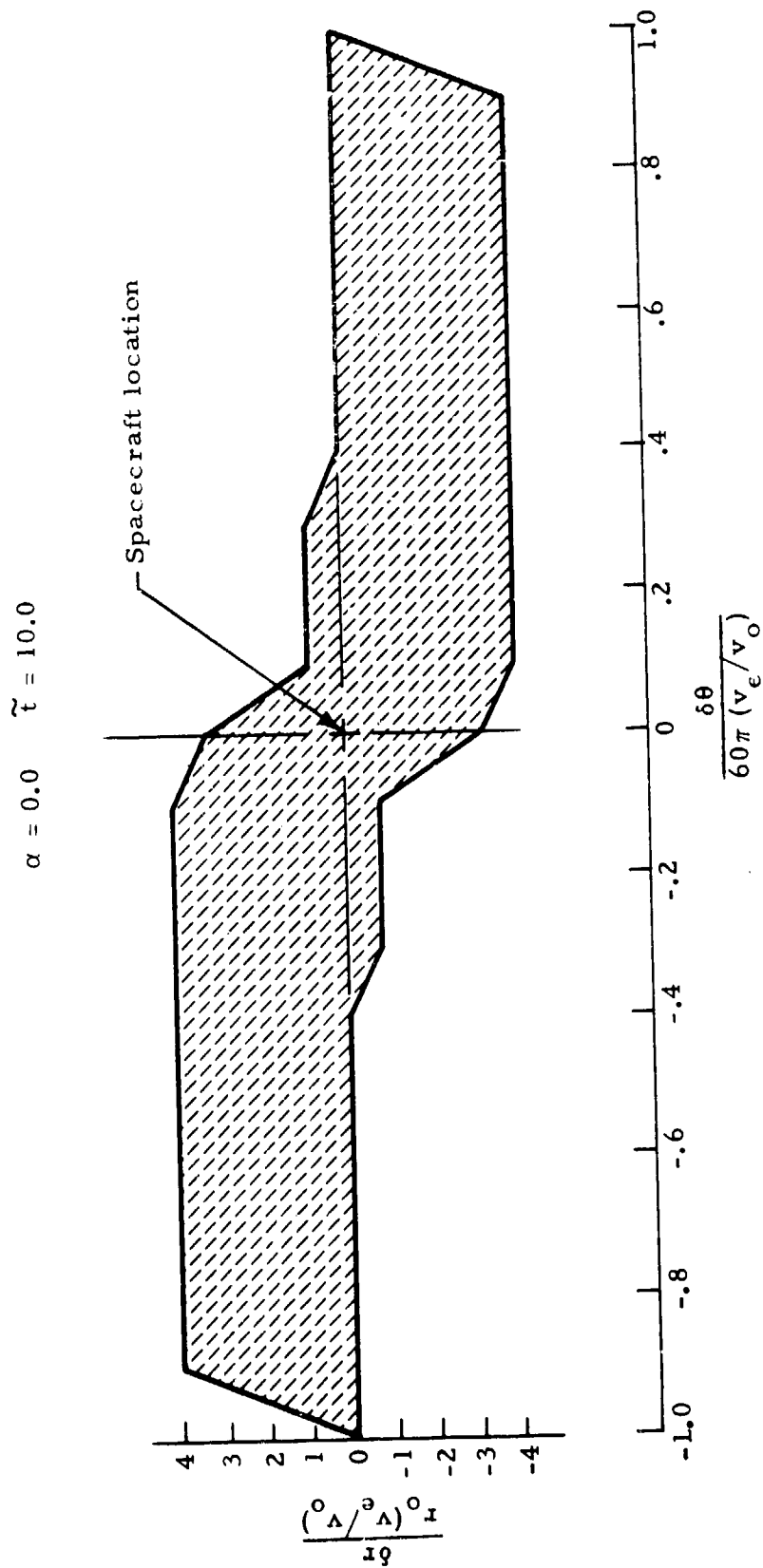Fig. 11 - Approximate Outline of Particle Cloud Projected onto the Spacecraft Orbit Plane (Aerodynamic Drag Neglected)
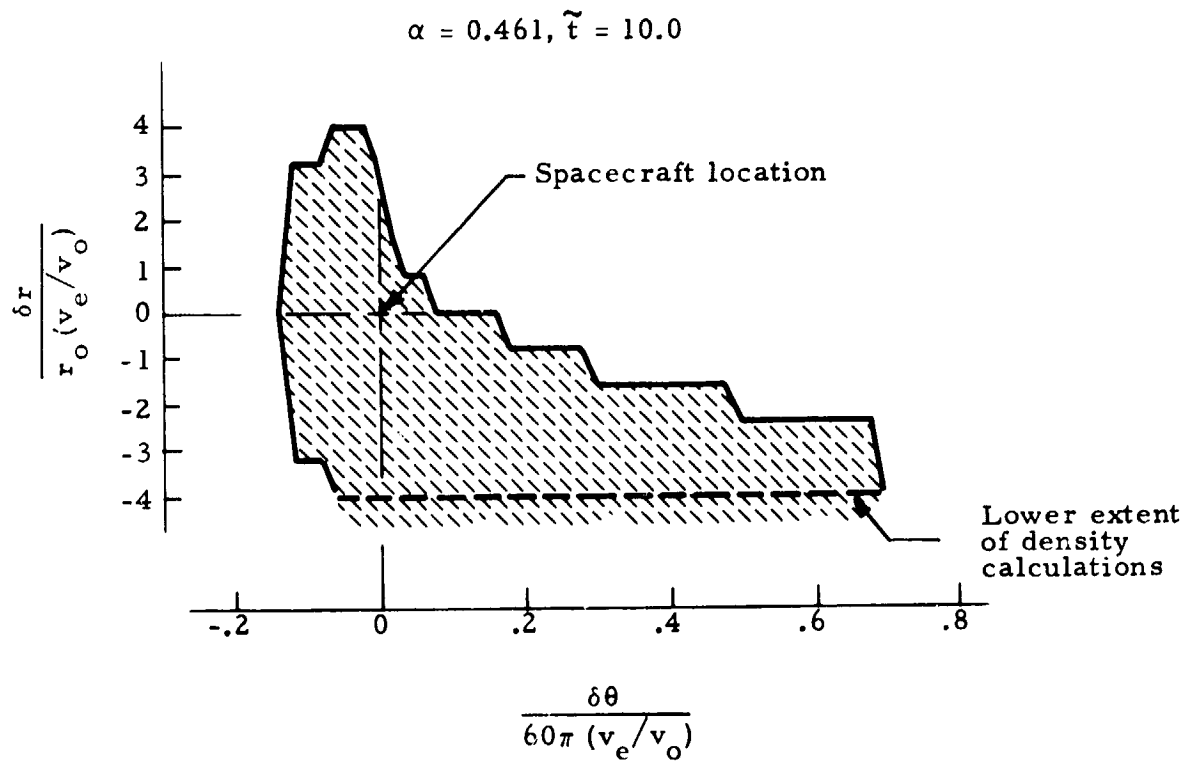
$\alpha = 0.461, \tilde{t} = 10.0$

Fig. 12 - Approximate Outline of Particle Cloud Projected
onto the Spacecraft Orbit Plane (Aerodynamic
Drag Included)

and spacecraft orbit parameters. The mesh parameters used in these calculations were M = 10 and N = 5, and the time step $\Delta \tilde{t}$ was 0.01. Recall that these calculations do not include particles in the source-flow phase of their trajectories (moving away from the spacecraft for the first time after having been ejected). The density field for an isotropic source is shown separately on the figures for comparison with the calculated results. The total density in the particle cloud is the sum of the two densities.

The data points in Figs. 5 through 8 did not show very much scatter, and so were simply connected by straight lines to display the overall trend. In Figs. 9 and 10, however, considerable scatter is present, and the trends are indicated by coarsly fairing the data using straight-line segments. This scatter in the data is evidently the result of numerical error stemming from the finite coarseness of the mesh and the finite time steps. By experimenting with the mesh and time step sizes, it was found that the scatter could be reduced. The computational costs increased, however, to the point that the increased accuracy was not economically justified. And, even with the data scatter, the overall trends seem quite clear and reasonable.

Figures 5 and 6 show that the density distribution in the radial direction (δ_r) maximizes and reaches an equilibrium after about six orbit periods for both the zero drag and finite drag cases. Aerodynamic drag is shown in Fig. 6 to shift the distribution toward the central body ($-\delta r$ direction).

The density distribution in the out-of-plane (ϕ) direction is shown in Figs. 7 and 8. Symmetry in the ϕ direction is shown to be unaffected by aerodynamic drag. The density level, however, is seen to be shifted down and smoothed out somewhat by the effects of drag. The downward shift at the spacecraft location is due to the overall shift of the cloud in the negative radial direction (Fig. 6). The slight peaking toward the edge shown in Fig. 7 is probably a computational anomaly caused by the finite grid mesh and time step.

The zero drag density distribution along the spacecraft orbit ($\delta\theta$ direction) is shown in Fig. 9 to maximize and reach an equilibrium at the spacecraft location; however, the extent of the distribution continues to expand in the positive and negative $\delta\theta$ directions. These observations are in accord with the behavior of the particle orbit equations. The effect of drag, as seen in Fig. 10, is to cause an equilibrium to be reached in the expansion of the cloud along the spacecraft orbit. Actually, the cloud will continue to expand, but it will simply spiral inward toward the central body and away from the spacecraft orbit.

The particle cloud shape was found to be symmetrical in the out-of-plane, ϕ, direction at all points ahead of and behind the spacecraft on the spacecraft orbit. As shown in Fig. 11 for zero drag, however, the shape is skewed with respect to the radial direction. Ahead of the spacecraft, the cloud shifts inward in the negative radial direction, while behind the spacecraft, the cloud shifts outward. Based on Eqs. (35) through (37), the particle cloud about the Skylab spacecraft (for zero drag) is found to extend, on both sides of the spacecraft, 35.6 km in the radial direction, 8.9 km in the out-of-plane direction and, after 10 orbits, 1680 km along the spacecraft orbit. In the absence of drag, the particle cloud would extend completely around the orbit and begin to overlap at the spacecraft location after 255 orbit periods.

A portion of the cloud shape for the case of aerodynamic drag is shown in Fig. 12. Calculations were not made beyond the lower extent shown.

3.3   COLUMN DENSITIES

Calculated values of column densities, normalized to the theoretical isotropic source value, are shown in Figs. 13 and 14. A value of $\tilde{R} = 1.12 \times 10^{-3}$ is used which is based on the Skylab spacecraft. These results are for lines of sight originating at the spacecraft location and extending in both directions along the r, θ and ϕ axes. The curvature of the orbit is not taken into

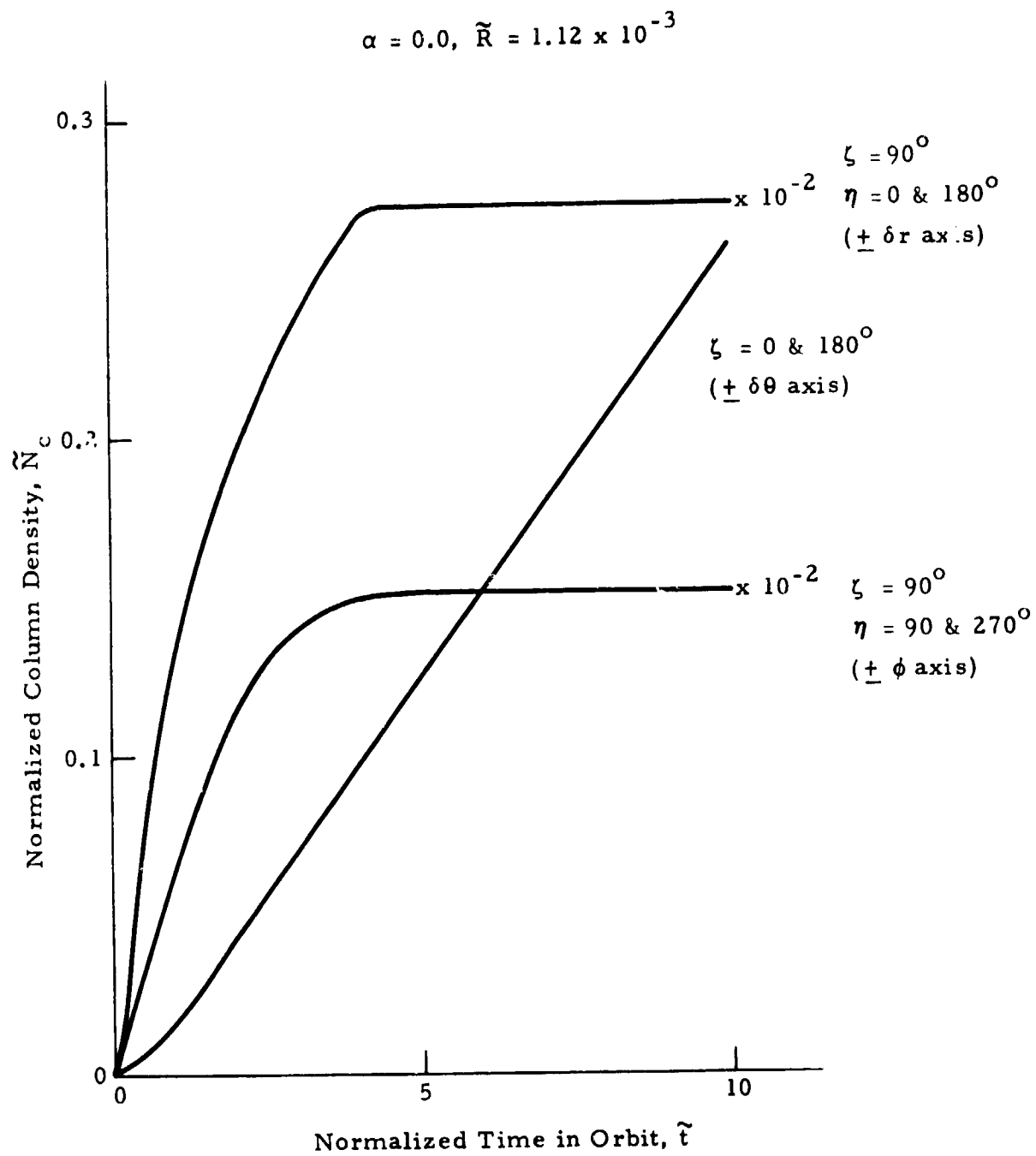$\alpha = 0.0, \ \widetilde{R} = 1.12 \times 10^{-3}$

Fig. 13 - Time Variation of Column Density Along Three Axes
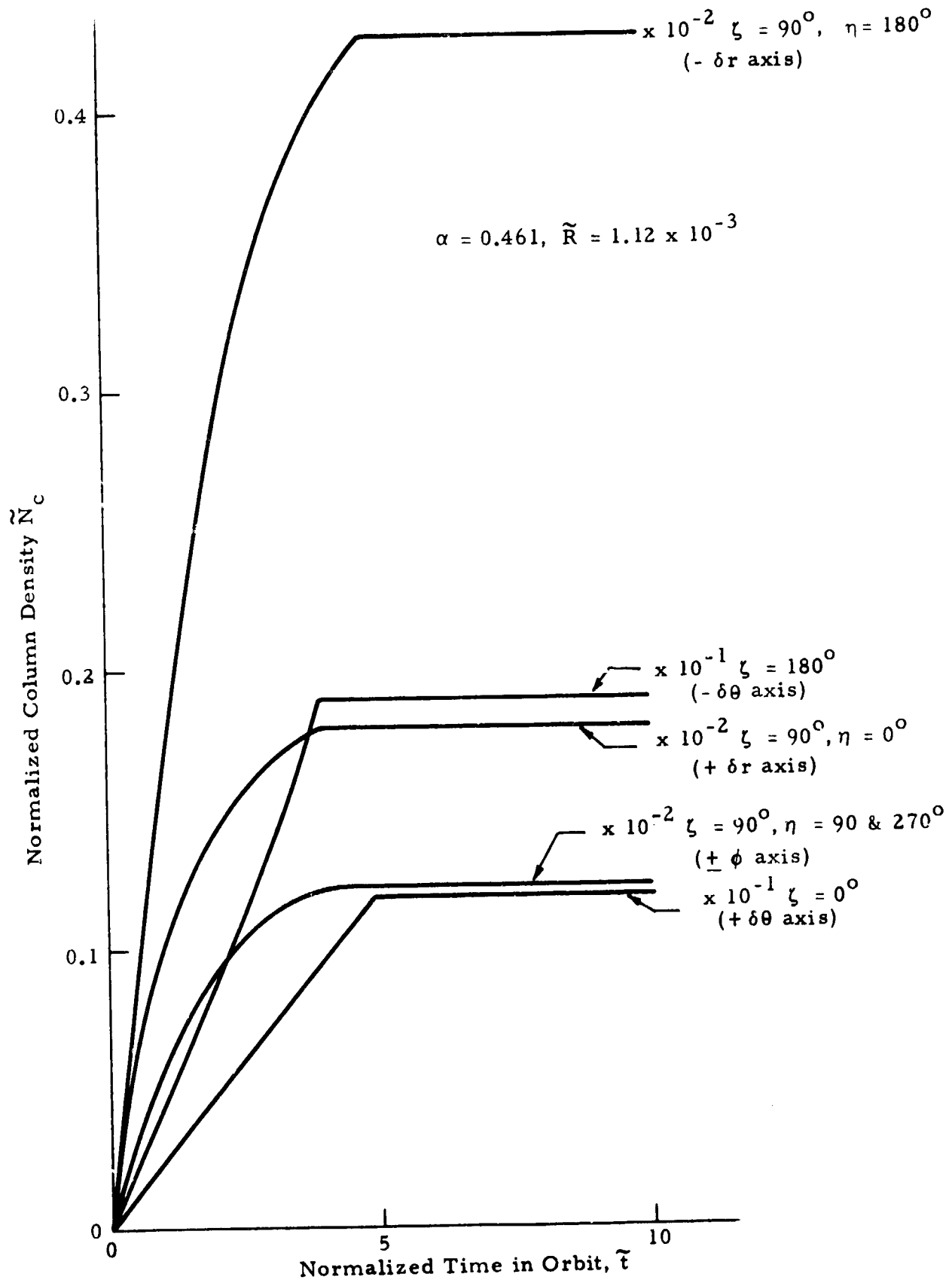(Aerodynamic Drag Neglected)

Fig. 14 - Time Variation of Column Density Along Three Axes
(Aerodynamic Drag Included)

account in these calculations. Also, the calculated column density values are based on the previously discussed cloud density calculations which do not include particles in the source flow portion of their trajectories.

Figure 13 shows that the zero drag column densities in the radial and out-of-plane directions (r and ϕ) reach an equilibrium after about five orbits. The equilibrium values are seen to be of the order of 10^{-3} of the theoretical isotropic source value. The column density in the direction along the orbit (θ) continues to increase as the cloud expands along the orbit. The curvature of the orbit, however, which is not taken into account in these calculations, will eventually bring about an equilibrium value in this direction also. For the Skylab spacecraft, the maximum line of sight distance, based on the cloud dimensions, is found to be about 2000 km. Using the maximum $\tilde{\rho}$ value of 27.5 in Figs. 5, 7 and 9 as the average along the line of sight, Eq. (50) yields an estimated maximum normalized column density $\tilde{N}_c$ of about 0.9. The actual value is certainly somewhat less than this estimation.

When drag is considered, the calculated column densities in all directions reach an equilibrium after about five orbits. These values are all seen to be of the order of 10^{-2} to 10^{-3} of the theoretical isotropic source value.

The results of the column density calculations show that the buildup of the particle cloud in orbit does not significantly affect column densities and, hence, light scattering and attentuation effects about the spacecraft. As pointed out in Section 2.4, the bulk of the column density for an isotropic source is concentrated within a few source radii, and the trapped particle cloud adds very little to that. For the case of zero drag, the trapped particle cloud effects are seen only within a narrow range in directions along the spacecraft orbit.

Section 4
CONCLUSIONS AND RECOMMENDATIONS

The results of this study effort show that a particle cloud does indeed build up about an orbiting spacecraft due to waste dumping, and a small fraction of this mass may return to the spacecraft after times corresponding to one half and one orbit period. The estimated return rate to the Skylab spacecraft, neglecting aerodynamic drag, was found to be of the same order as the outgas rate of a typical spacecraft material. When drag was considered, however, the particle orbits were found to decay away from the spacecraft orbit such that no collisions with the spacecraft were possible.

The trapped particle cloud was found to contribute very little to light scattering and attenuation effects, as predicted by calculated column densities, when compared with the source flow region near the spacecraft. The bulk of the column density along a line of sight originating at the spacecraft is concentrated within a few spacecraft radii. Some intensification of these effects, however, is found in directions along the spacecraft orbit.

The analysis reported herein utilized certain simplifying assumptions, such as a uniform distribution of particle sizes and expulsion velocities, a constant and uniform expulsion rate and spherical symmetry in the direction of expulsion. Moreover, the particles were not considered to evaporate or otherwise be altered over a period of time. Future effort in this area should include removing some of the restraints in these assumptions and possibly considering the long-term interaction and thermal equilibrium of these particles with the ambient atmosphere.

4-1

Section 5
REFERENCES

1. Greenwood, D.T., Principles of Dynamics, Prentice-Hall, Inc., Englewood Cliffs, N.J., 1965.

2. Shrodt, J., "ATM Contamination Follow-On Study," Vol.II, TN 67-68, Ball Brothers Research Corporation, Boulder, Colo., 28 October 1967.

Appendix

COMPUTER PROGRAM

Appendix

The computer program used in the particle cloud analysis is listed in the following pages. This program was developed for use on the NASA-MSFC Univac 1108 system. The input and output variables are described as follows:

Input Variables

M	M in Section 2.3
N	N in Section 2.3
A	α in Section 2.1
TMAX	$\tilde{t}_{max}$ in Section 2.3
DELT	$\Delta\tilde{t}$ in Section 2.3
TWRT	instructs program to write output variables at $\tilde{t} = n$ TWRT, $n = 1, 2, \ldots$
R	$\tilde{R}$ in Section 2.2

Output Variables

F	$\mathscr{F}_i$ in Section 2.3
FO	$\mathscr{F}_o$ in Section 2.3
I	i in Section 2.3
IP, JP, KP	i', j', k' in Section 2.3
DEN	$\tilde{\rho}$ in Section 2.3
ME	M_η in Section 2.3
T	$\tilde{t}$ in Section 2.1
COLDEN	$\tilde{N}_c$ in Section 2.4
ETA	η in Section 2.1
ZETA	ζ in Section 2.1

LMSC-HREC D306222

PROGRAM LISTING

```
      DIMENSION F(100),ME(100)
      COMMON T,TMAX,ST,CT,FXPT,A,SZ,CZ,SE,CE,PI,DR,DTH,PHI
     *,DEN(10,100,10),N,NP,FI,DELT,N2N,N2NP,DLDNP,DEL,DELJ
     *,RPMAX,RPMIN,THTMAX,THTMIN,PHIMAX,PHIMIN
      READ(5,10,END=999)M,N,A,TMAX,DELT,TWRT,R
      WRITE(6,20)M,N,A,TMAX,DELT,TWRT,R
10 FORMAT(I5,I5,F10.4,3F10.3 ,F10.4)
20 FORMAT(//5X2HM=I3,2X2HN=I3,2X2HA=E10.4,2X5HTMAX=F7.2,2X5HDELT=
     * F5.2,2X5HTWRT=F5.2,2X2HR=F10.4)
      PI=3.14159265
      TCK=TWRT-0.5*DELT
      NP=IFIX(TMAX*FLOAT(N))
      N2N=2*N-1
      N2NP=2*NP-1
      M2=2*M
      DLDNP=8.0*FLOAT(N**3)*DELT
      DELZ=PI/FLOAT(2*(M+1))
      DEL=1.0/FLOAT(N)
      DELJ=1.0/FLOAT(NP)
      RPMAX=(FLOAT(N)-0.5)*DEL
      RPMIN=-RPMAX
      THTMAX=(FLOAT(NP)-0.5)*DELJ
      THTMIN=-THTMAX
      PHIMAX=RPMAX
      PHIMIN=-PHIMAX
      COSI=COS(DELZ)
      FO=0.5*(1.0-COSI)
      WRITE(6,33)FO
33 FORMAT(//2X3HFO=F12.4)
      DO 30 I=1,M
      COSIP1=COS(FLOAT(I+1)*DELZ)
      X1=COSI-COSIP1
      X2=X1/(2.0*FO)
      ME(I)=IFIX(X2)
      MET=IFIX(X2+0.5)
      IF(MET.GT.ME(I))ME(I)=MET
      F(I)=X1/FLOAT(2*ME(I))
30 COSI=COSIP1
      WRITE(6,34)
34 FORMAT(//4X1HI,3X2HME,6X1HF//)
      WRITE(6,35)(I,ME(I),F(I),I=1,M)
35 FORMAT(2I5,F12.4)
      T=0.3
      DO 40 I=1,N2N
      DO 40 J=1,N2NP
      DO 40 K=1,N2N
40 DEN(I,J,K)=0.0
100 TP=2.0*PI*R
      ST=SIN(TP)
      CT=COS(TP)
      FXPT=EXP(-A*T)
      FI=FO
      SZ=0.0
      CZ=1.0
      SE=0.0
      CE=1.0
      CALL POS
      CALL DENS
```

6-2

```
      DO 200 I=1,MP
      Z=(FLOAT(I)+0.5)*DELZ
      SZ=SIN(Z)
      CZ=COS(Z)
      IF(I.GT.M)GO TO 150
      MEP=MF(I)
      FI=F(I)
      GO TO 160
150   MEPP=MP-I+1
      MEP=MF(MEPP)
      FI=F(MEPP)
160   DELE=2.0*PI/FLOAT(MEP)
      DO 200 J=1,MEP
      E=(FLOAT(J)-0.5)*DELE
      SE=SIN(E)
      CE=COS(E)
      CALL POS
200   CALL DENS
      FI=FO
      SZ=0.0
      CZ=-1.0
      SE=0.0
      CE=1.0
      CALL POS
      CALL DENS
      IF(T.LT.TCK)GO TO 400
      TCK=TCK+TWRT
      WRITE(6,250)T
250   FORMAT(//10X2HT=F8.2)
      DO 300 JP=1,N2NP
      WRITE(6,251) JP
251   FORMAT(/5X3HJP=I3/)
      DO 300 KP=1,N2N
300   WRITE(6,301)(DEN(IP,JP,KP),IP=1,N2N)
301   FORMAT(10E12.4)
      C=PI*R*24.0/FLOAT(N)
      C1=C*6.0*PI
      COLDEN=C1/2.0*DEN(N,NP,N)
      NPP=NP+1
      DO 600 J=NPP,N2NP
600   COLDEN=COLDEN+C1*DEN(N,J,N)
      WRITE(6,602)COLDEN
602   FORMAT(//5X6HZETA=0,2X7HCOLDEN=F12.4)
      COLDEN=C1/2.0*DEN(N,NP,N)
      NPP=NP-1
      DO 610 J=1,NPP
610   COLDEN=COLDEN+C1*DEN(N,J,N)
      WRITE(6,612)COLDEN
612   FORMAT(//5X12HZETA=180 DEG,2X7HCOLDEN=F12.4)
      C1=4.0*C
      COLDEN=C1/2.0*DEN(N,NP,N)
      NPP=N+1
      DO 620 I=NPP,N2N
620   COLDEN=COLDEN+C1*DEN(I,NP,N)
      WRITE(6,622)COLDEN
622   FORMAT(//5X17HZETA=90 DEG,ETA=0,2X7HCOLDEN=F12.4)
      COLDEN=C1/2.0*DEN(N,NP,N)
      NPP=N-1
```

6-3

```
      DO 630 I=1,NPP
630  COLDEN=COLDEN+C1*DEN(I,NP,N)
      WRITE(6,632)COLDEN
632  FORMAT(//5X23HZETA=90 DEG,ETA=180 DEG,2X7HCOLDEN=E12.4)
      COLDEN=C/2.0*DEN(N,NP,N)
      NPP=N+1
      DO 640 K=NPP,N2N
640  COLDEN=COLDEN+C*DEN(N,NP,K)
      WRITE(6,642)COLDEN
642  FORMAT(//5X22HZETA=90 DEG,ETA=90 DEG,2X7HCOLDEN=E12.4)
      COLDEN=C/2.0*DEN(N,NP,N)
      NPP=N-1
      DO 650 K=1,NPP
650  COLDEN=COLDEN+C*DEN(N,NP,K)
      WRITE(6,652)COLDEN
652  FORMAT(//5X23HZETA=90 DEG,ETA=270 DEG,2X7HCOLDEN=E12.4)
400  T=T+DELT
      IF(T.LT.TMAX) GO TO 100
999  STOP
      END


      SUBROUTINE POS
      COMMON T,TMAX,ST,CT,EXPT,A,SZ,CZ,SE,CE,PI,DR,DTH,PHI
     *,DEN(10,100,10),N,NP,FI,DELT,N2N,N2NP,DLDNP,DEL,DELJ
     *,RPMAX,RPMIN,THTMAX,THTMIN,PHIMAX,PHIMIN
      DR=0.25*((SZ*CE+A/PI))*ST+2.0*CZ*(1.0-CT)-2.0*A*T)
      DTH=-CZ*T/TMAX+0.5*A*T**2/TMAX-1.0/(3.0*PI*TMAX)*((SZ*CE+A/PI)*
     * (1-CT)-2.0*CZ*ST)
      PHI=SZ*SE*ST
      RETURN
      END


      SUBROUTINE DENS
      COMMON T,TMAX,ST,CT,EXPT,A,SZ,CZ,SE,CE,PI,DR,DTH,PHI
     *,DEN(10,100,10),N,NP,FI,DELT,N2N,N2NP,DLDNP,DEL,DELJ
     *,RPMAX,RPMIN,THTMAX,THTMIN,PHIMAX,PHIMIN
      LOGICAL L1,L2,L3
      L1=DR.GT.RPMAX.OR.DR.LT.RPMIN
      L2=DTH.GT.THTMAX.OR.DTH.LT.THTMIN
      L3=PHI.GT.PHIMAX.OR.PHI.LT.PHIMIN
      IF(L1.OR.L2.OR.L3)GO TO 100
      TCKP=TMAX-0.5*DELT
      IF(T.GT.TCKP)GO TO 5
      IT=IFIX(T)+1
      NIT1=NP-N*IT+1
      NIT2=NP+N*IT-1
      GO TO 8
5    NIT1=1
      NIT2=N2NP
8    CONTINUE
      DO 10 I =1,N2N
      RP=(FLOAT(I-N)+0.5)*DEL
      IF(DR.GT.RP) GO TO 10
      IP=I
      GO TO 15
10   CONTINUE
15   DO 20 J=NIT1,NIT2
      THP=(FLOAT(J-NP)+0.5)*DELJ
```

LMSC-HREC D306222

```
      IF(DTH.GT.THP)GO TO 20
      JP=J
      GO TO 25
  20  CONTINUE
  25  DO 30 K =1.N2N
      PHIP=(FLOAT(K-N)+0.5)*DFL
      IF(PHI.GT.PHIP)GO TO 30
      KP=K
      GO TO 35
  30  CONTINUE
  35  DEN(IP,JP,KP)=DEN(IP,JP,KP)+DLDNP*FI
 100  CONTINUE
      RETURN
      END
```